International Journal of Hydrogen Energy

Mechanistic studies of lower temperature isomerization of n-heptane over fibrous silica molybdenum catalyst

--Manuscript Draft--

Manuscript Number:	HE-D-22-08512R1
Article Type:	SI:WHEC2022-H2 Economy (Chen)
Section/Category:	Catalysts / Electrocatalysts / Photocatalysts
Keywords:	n-C7 isomerization; MoO3-based catalysts; Platinum; Lewis acid; Protonic acid side
Corresponding Author:	A.A. Jalil, Ph.D Johor Bahru, MALAYSIA
First Author:	A.A. Jalil, Ph.D
Order of Authors:	A.A. Jalil, Ph.D
	M.B. Bahari
	N.S. Hassan
	M.H. Razak
	N.M. Izzudin
	M.A.A. Aziz
	N.F. Khusnun
	M.A.H. Aziz
	A.F.A. Rahman
	W. Nabgan
	Saravanan Rajendran
	C.R. Mamat
Abstract:	Platinum (Pt) inclusion on fibrous silica molybdenum (FSMO) and MoO3/KCC-1 catalysts has been prepared and utilized for the lower temperature (200-350 ºC) catalytic isomerization of n-heptane. The impact of Pt inclusion towards the structure, morphology, and acid distribution of catalysts was characterized by XRD, FTIR, N2-physisorption, Py-IR, and H2-IR. Compared with MoO3/KCC-1, FSMO demonstrated superior MoO3 dispersion and amount of Lewis acid site associated with the in-situ synthesis technique. Although Pt inclusion slightly lessened acid sites due to inevitable partial coverage by the Pt cluster, the considerably higher amount of Lewis acid sites compared to Brønsted and conjugated sufficiently for generating protonic acid sites for enriching the isomerization activity. In contrast to Pt/MoO3/KCC-1 and undoped catalysts, Pt/FSMO achieved a superior conversion of 70.9% with 63.6% isomer yield at a low temperature of 250 ºC. The 28-h stability tests demonstrated that Pt/FSMO recorded stable isomerization activity, with a superior isomer yield (~48-52%) and inferior cracking yield (<3.0%) than Pt/MoO3/KCC-1.

Aishah Abdul Jalil (Ph.D)
Centre of Hydrogen Energy
Institute of Future Energy
Faculty of Chemical and Energy Engineering
Universiti Teknologi Malaysia
81310 UTM Johor Bahru
Johor.

05 MARCH 2023

Editor in Chief,
International Journal of Hydrogen Energy

Dear Prof,

Manuscript ID: HE-D-22-08512

Thank you very much for reviewing our manuscript and allowing us to revise the manuscript entitled "**Mechanistic studies of lower temperature isomerization of n-heptane over fibrous silica molybdenum catalyst**". We are also grateful to the reviewers for the helpful comments. The manuscript has been revised after carefully considering the comments.

As described in the following pages, all the comments are addressed clearly and appropriately. In addition, some corrections have been made. All the changes are highlighted in yellow, as provided in the revised manuscript. We believe the revised manuscript is now acceptable for publication in the *International Journal of Hydrogen Energy*.

Thank you again for your time and consideration of this manuscript.

Sincerely yours,
Aishah Abdul Jalil (Ph.D)

Suggested Reviewer:

C.K. Cheng, PhD
Associate Professor, Khalifa University of Science Technology - Abu Dhabi Campus:
Khalifa University of Science and Technology
cheng.kui@ku.ac.ae
An expert in catalysts and catalysis.

H.D. Setiabudi, PhD
Associate Professor, Universiti Malaysia Pahang
herma@ump.edu.my
An expert in catalysts and catalysis.

Ankit kumar
Department of Chemical Engineering and Technology, Indian Institute of Technology (BHU),
Varanasi, UP, 221005, India
ankit.rs.che14@iitbhu.ac.in
An expert in catalytic and catalysis

S.H. Zein PhD
Associate Professor, School of Chemical Engineering, Universiti Sains Malaysia
chhussein@eng.usm.my
An expert in heterogenous catalysis

RESPONSE TO REVIEWERS

Manuscript Reference Number: HE-D-22-08512

Title: Mechanistic studies of lower temperature isomerization of n-heptane over fibrous silica molybdenum catalyst

The authors would like to appreciate the valuable comments from reviewers for improving our manuscript.

Reviewer #1

Comment 1:

What is the meaning of the word "Mechanistic" (in title of the article) in relation to this study?

Author reply:

In the context of our study, the term "mechanistic" refers to the investigation and understanding of the specific chemical reactions and steps that occur during the lower-temperature isomerization of n-C_7 over the FSMO. This involves identifying the intermediate species, reaction pathways, and the role of the catalyst in promoting the desired reaction. Essentially, our work proposed the underlying mechanisms that govern the n-C_7 isomerization process over FSMO, which is essential for optimizing the catalyst performance and designing more efficient and selective catalysts.

Comment 2:

In the experimental part, it's not quite clear at what stage of the synthesis molybdenum is added to the FSMO sample.

Author reply:

Thank you for the comment. The authors would like to apologize for the missing information. The authors already added the missing information in the experimental part, as highlighted in the revised manuscript.

"Thereafter, butanol and toluene were poured into the mixture under continuous agitation at ambient temperature before being dopped with the specified amount of MoO_3 seed." -Lines 113-115

Comment 3:

In the same part, the amount of molybdenum and platinum introduced into the catalysts should be indicated.

Author reply:

Thank you for the comment. In this work, the authors utilized molybdenum and platinum precursor to attain 10.0 wt%MoO_3 and 0.1 wt%Pt, respectively, during the synthesis Pt/FSMO and MoO_3/KCC-1 catalysts. As highlighted in the revised manuscript, the amount of molybdenum and platinum introduced into the catalysts has been added in the experimental part.

"For KCC-1 supported 10.0 wt%MoO_3 catalyst," -Line 124

"as the metal precursor (0.1 wt%Pt) over FSMO support" -Line 130

Comment 4:

Lines 214-215 the meaning of the sentence needs to be clarified - it seems that the meaning should be reversed. Since it is not the relative pressure of N_2 uptakes increased, but an increase in N_2 uptake at higher relative pressures.

Author reply:

Thank you for the comment. As advised, the authors have already rewritten the sentences as highlighted in the revised manuscript.

"However, when Pt was loaded onto the catalyst surface, the N_2 uptakes for Pt/MoO_3/KCC-1 increased substantially at higher relative pressure, while Pt/FSMO catalyst demonstrated an insignificant change." -Lines 216-218

Comment 5:

How was the average pore size calculated, which is presented in table 1? (it is desirable to clarify the formulas).

Author reply:

The authors want to sincerely apologize since we could not prove the calculation for the average pore size. The average pore size in Table 1 was measured by using BJH (Barrett-Joyner-Halenda) approach, automatically generated by the Beckman Coulter SA3100 unit. Based on the literature, the pore size distribution data were initially obtained using the BJH method. Then, the average pore diameter can be calculated by integrating the pore size distribution over the entire range of pore sizes and dividing it by the total pore volume. The equation for calculating the average pore diameter using the BJH method is:

$$\text{Average pore diameter} = \int D*PSD(D)dD \,/\, \int PSD(D)dD$$

where D is the pore diameter and PSD is the pore size distribution.

Comment 6:

Fig 3b: y-axis for pore size distribution curves usually show dV/dr or dV/dD. Please explain why it is marked as dV/dp, what does "dp" mean? Also in the numerator is the change in pore volume, so the dimension should not be negative for "cm3" (cm3nm-1g-1).

Author reply:

Thank you for the comment. The authors want to apologize for our careless mistake. The authors agreed that in Fig 3b, the y-axis for pore size distribution curves should be "dV/dD", while the unit in "$cm^3\ nm^{-1}\ g^{-1}$". Thus, the authors replaced the figure with the correct version, as provided in the List of Figures.

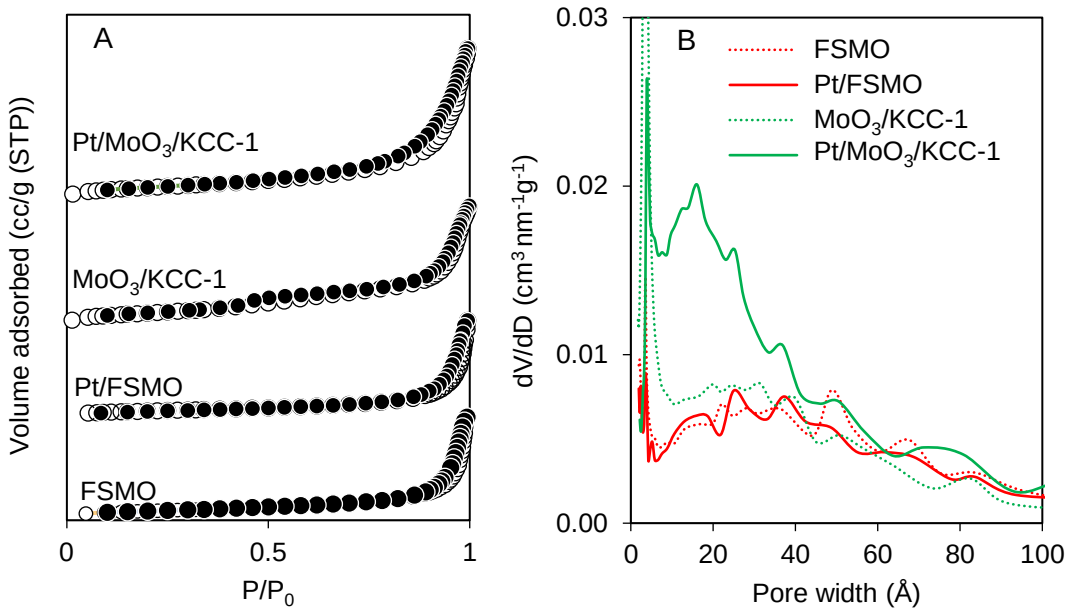

Fig. 3 N_2 adsorption-desorption and pore distribution for MoO_3-based catalysts

Comment 7:

According to IR studies (Figures 5-6): were extinction coefficients taken into account when calculating the number of BAS and LAS?

Author reply:

No. The authors only determine the qualitative presence or absence of basic and acidic sites on the surface of a material based on the intensity of the corresponding peaks.

Comment 8:

The reaction conditions (temperature, pressure, catalysts loading, molar ratio of hydrogen to n-heptane, raw material feed rate) should be indicated when studying the stability of catalysts (Fig. 8).

Author reply:

Thank you for the comment. As advised, the authors provided the reaction condition for the stability test in the caption for Fig. 8, as highlighted in the revised List of Figures.

Fig. 8 Catalyst stability test under 28 h time-on-stream at 250 ºC, atmospheric pressure, and 0.2 g of catalyst. (2 µmol of n-C_7 + 100 ml min^{-1} H_2)

Comment 9:

What explains the lower conversion of heptane at temperatures of 200 and 350°C for the sample with platinum (Pt/FSMO), compared to the sample without platinum (FSMO, Fig. 7)?

Author reply:

According to Ibrahim et al. (2020), the moderate Brønsted acid sites and abundant Lewis acid sites favours hydroisomerization, explaining the enhancement in the catalytic performance of Pt/HM@KCC-1. Regarding to this work, as seen in Fig. 7, although Pt/FSMO possessing abundant Lewis acid sites compared to FSMO, the inferior amount of Brønsted acid sites could explaining the lower conversion of heptane at temperatures of 200 °C. Similar phenomenon also occur at 350°C, which inferior amount of Brønsted and Lewis acid sites recorded for Pt/FSMO over FSMO.

References:

Ibrahim, M., Jalil, A. A., Khusnun, N. F., Fatah, N. A. A., Hamid, M. Y. S., Gambo, Y., Abdulrasheed, A. A., Hassan, N. S. (2020). Enhanced n-hexane hydroisomerization over bicontinuous lamellar silica mordenite supported platinum (Pt/HM@ KCC-1) catalyst. International Journal of Hydrogen Energy, 45(36), 18587-18599.

Comment 10:

It would be interesting to determine the coke content on the surface after 28 hours of testing Pt-FSMO and Pt/MoO3/KCC-1 samples (Fig. 8).

Author reply:

Thank you for the comment. As requested, the authors have already added the temperature-programmed oxidation analysis to determine the coke content on the surface after 28 hours of testing Pt-FSMO and Pt/MoO3/KCC-1 samples, as highlighted in the revised manuscript.

Temperature-programmed oxidation (TPO) was carried out in Mettler Toledo TGA/SDTA/851e Thermo-gravimetric unit to estimate the carbonaceous deposition on the surface of spent catalysts within the temperature of 10-900 °C. Lines-154-156

The temperature-programmed oxidation analysis was conducted to quantify the extent of carbonaceous deposition on the spent catalysts. As depicted in Fig. S1, it was evidenced that Pt/FSMO possessed an inferior amount of coke compared to Pt/MoO_3/KCC-1, further proving the stability of isomerization activity within 28 h reaction. Lines 347-350

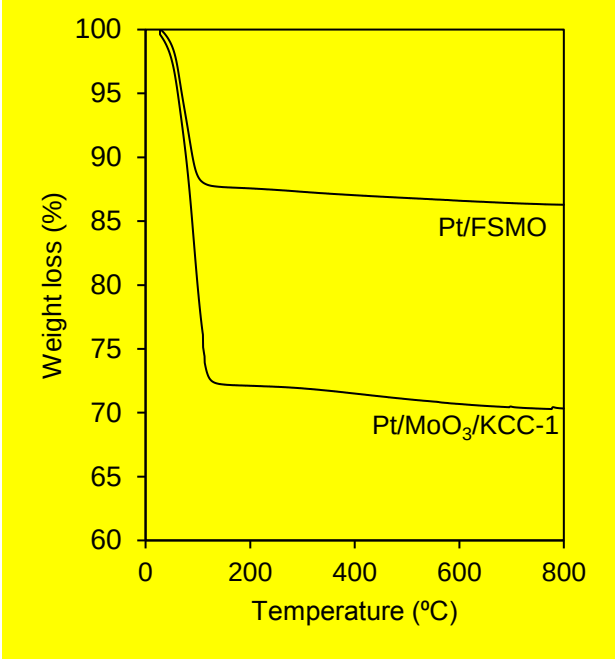

Fig. S1 TPO profile of spent Pt/FSMO and Pt/MoO_3/KCC-1 after catalyst stability test under 28 h time-on-stream at 250 ºC

Comment 11:

Throughout the text of the article, there are two ways of writing of the fibrous silica molybdenum catalyst sample - FSMO and FSMo. In addition, there is a typo in line 352 - $FSMO_3$.

Author reply:

Thank you for the comment. The authors want to apologize for our mistake. The authors already rewrite the term used for fibrous silica molybdenum catalyst "FSMO" in the whole manuscript, as highlighted in the revised manuscript.

"fibrous structure of support with silica (FSMO)," – Line 353

Comment 12:

Line 427 - "isomerisation", in the rest of the text - "isomerization".

Author reply:

We want to apologize for our mistake. The authors already replaced "isomerisation" with "isomerization", as highlighted in the revised manuscript.

"Thus, isomerization activity improved, especially at the lower reaction temperature."-Line 428

Comment 13:

Lines 447 and 448 - need to make a subscript for the formula "MoO3".

Author reply:

We want to apologize for our mistake. The authors already make a subscript for the formula "MoO_3", as highlighted in the revised manuscript.

"compared to MoO_3/KCC-1, regardless of" -Lines 448-449

Comment 14:

For the entire list of references, it is necessary to check the subscripts in chemical formulas. Also note that there is not enough data for reference [37] (volume number, page number).

Author reply:

We want to apologize for our mistake. The authors already checked all the subscripts issues in references and provided the volume number, page number for reference [37], as highlighted in the revised manuscript.

[37] Azami MS, Jalil AA, Aziz FFA, Hassan NS, Mamat CR, Izzudin NM. Influence of the nitrogen pots from graphitic carbon nitride with the presence of wrinkled silica-titania for photodegradation enhancement of 2-chlorophenol. International Journal of Hydrogen Energy. 2021;48:6532-6545.

[38] Aziz FFA, Jalil AA, Triwahyono S, Mohamed M. Controllable structure of fibrous SiO_2–ZSM-5 support decorated with TiO_2 catalysts for enhanced photodegradation of paracetamol. Applied Surface Science. 2018;455:84-95.

Comment 15:

Line 162 - written "n-C5" instead "n-C7".

Author reply:

We want to apologize for our careless mistake. The authors already replaced "n-C_5" with "n-C_7", as highlighted in the revised manuscript.

"about two µmol of n-C_7 was driven into" - Line 165

Comment 16:

Line 165 - temperature is given in kelvins (77 K), while the rest of the text uses degrees Celsius.

Author reply:

Thank you for the comment. The authors already replaced temperature unit "77" with "-196 °C", as highlighted in the revised manuscript.

"The isomerization product was confined using N_2 (-196 °C)" - Line 165

Comment 17:

Line 297 - please clarify "-H" is a hydride ion designation?

Author reply:

Thank you for the comment. We want to apologize for our mistake. That "-H" corresponds to the hydrogen atom from the Si-OH bond. The incorporation of MoO_3 in the fibrous silica framework resulted in more hydrogen atom replacement by Mo ions to form Si-O-Mo, associated with the alternately aligned SiO_2 and MoO_3 in the fibrous structure compared to MoO_3/KCC-1. In order to avoid confusion, the author already replaced "-H" with "hydrogen atom", as highlighted in the revised manuscript.

"there was more replacement of hydrogen atom (from Brønsted Si-OH) by Mo ions in forming Si-O-Mo (Lewis acid sites)." - Line 298

Comment 18:

It is need to specify decryption for Yhhc (figs. 7, 8).

Author reply:

Thank you for the comment. As advised, the authors added the description for Yhhc in the figure caption, as highlighted in the revised List of Figures.

"**Fig. 7** *n*-heptane isomerization activity over MoO_3-based catalyst at elevated temperature (Y_{iso}= yield of isomer, $Y_{cracking}$ = Yield of cracking, and Y_{hhc} = Yield of higher hydrocarbon)"

Reviewer #2

Comment 1:

Line 159: Why is oxygen stream used? What is the need for this work?

Author reply:

Thank you for the comment. The purpose of treating the tested catalyst with oxygen is to remove any impurities or residues that may be present on the surface of the catalyst. These impurities can interfere with the activity and selectivity of the catalyst during the reaction.

Comment 2:

Line 162: Why was normal pentane (n-C5) injected into the reactor? Unless the isomerization of normal heptane is not the goal of the work?

Author reply:

The authors would like to apologize for our careless mistake. The authors already replaced "n-C_5" with "n-C_7", as highlighted in the revised manuscript.

"about two µmol of n-C_7 was driven into" - Line 165

Comment 3:

Line 165: What is the need to use nitrogen carrier gas to transfer products to GC? In this way, it seems that at the used temperature, the products are completely gaseous, and if GC Online is used, the products are injected into it online.

Author reply:

Thank you for the comment. In this work, the authors did not use nitrogen as a carrier to transfer the products to GC. The outlet stream was immersed in liquid nitrogen before flash-evaporating into the gas chromatograph system. This approach was applied because of:

i) The low temperature of liquid nitrogen helps to quench the isomerization reaction, stopping any further changes to the product. This part is important because

isomerization reactions can be temperature-sensitive and may continue to occur even at lower temperatures.

ii) The cold temperature of liquid nitrogen also helps to condense and remove any volatile impurities or byproducts that may have formed during the reaction. This condition helps to ensure that only the desired product is analyzed in the gas chromatograph system, improving the accuracy and precision of the analysis.

Finally, the flash-evaporation of the isomerization product from the liquid nitrogen into the gas chromatograph system ensures that the sample is quickly vaporized and carried by the carrier gas through the column for separation and detection. This step is crucial because it helps to minimize any potential losses or degradation of the sample during the sample introduction process.

Comment 4:

It is necessary to state the information of GC used.

Author reply:

Thank you for the comments. The information on GC used in this isomerization work has already been mentioned in the experimental part. The authors used an online 6090 N Agilent gas chromatograph equipped with HP-5 Capillary Column and FID detector to analyse the isomerization product.

"An online gas chromatograph (Agilent 6090N, FID, HP-5), connected with a utilized micro-catalytic pulse reactor, scrutinized the isomerization product." Lines 164-165

Comment 5:

Line 169: The definition of selectivity used does not seem to be correct. Refer to the references and use a better definition for selectivity.

Author reply:

Thank you for the comment. The authors would like to apologize for our mistake. The formula with the definition used to estimate the isomerization activity was rewritten, as highlighted in the revised manuscript.

$$X_i(\%) = \frac{\sum A_i - A_{r,i}}{\sum A_i} \times 100\% \quad (1)$$

$$S_i(\%) = \frac{A_i}{\sum A_i - A_{r,i}} \times 100\% \quad (2)$$

$$Y_i = \frac{X_i \times S_i}{100} \quad (3)$$

Where A_i = corrected chromatographic area for a specific product and $A_{r,i}$ = corrected chromatographic area for residual of n-heptane species, in weight percent unit.

References:

[1] Setiabudi, H. D., Jalil, A. A., Triwahyono, S., Kamarudin, N. H. N., & Mukti, R. R. (2012). IR study of iridium bonded to perturbed silanol groups of Pt-HZSM5 for n-pentane isomerization. Applied Catalysis A: General, 417, 190-199.

[2] Ruslan, N. N., Fadzlillah, N. A., Karim, A. H., Jalil, A. A., & Triwahyono, S. (2011). IR study of active sites for n-heptane isomerization over MoO3-ZrO2. Applied Catalysis A: General, 406(1-2), 102-112.

Comment 6:

What percentage of metals (platinum and molybdenum) have been used to prepare the catalysts? Why?

Author reply:

Thank you for the comment. In this work, the authors utilized molybdenum and platinum precursor to attain 10.0 wt%MoO_3 and 0.1 wt%Pt, respectively, during Pt/FSMO and MoO_3/KCC-1 catalysts preparation. As highlighted in the revised manuscript, the amount of molybdenum and platinum introduced into the catalysts has been added.

"For KCC-1 supported 10.0 wt%MoO_3 catalyst," -Line 124

"as the metal precursor (0.1 wt%Pt) over FSMO support" -Line 130

- 0.1 wt%Pt was applied since several studies claimed that adding 0.1% of Pt increases activity and stability during isomerization. However, the increase in Pt content resulted in a decrement in isomerization activity

References:

[1] Grau, J. M., Yori, J. C., & Parera, J. M. (2001). Hydroisomerization–cracking of n-octane on Pt/WO42−–ZrO2 and Pt/SO42−–ZrO2: Effect of Pt load on catalyst performance. Applied Catalysis A: General, 213(2), 247-257.

[2] Yang, L., Song, Z., Yu, Y., Zhu, L., & Xia, D. (2020). Bimetallic bifunctional Pt-NiP/Hβ as a novel and highly efficient catalyst for n-hexane isomerization. Catalysis Surveys from Asia, 24, 104-114.

[3] Zhang, A., Nakamura, I., Aimoto, K., & Fujimoto, K. (1995). Isomerization of n-pentane and other light hydrocarbons on hybrid catalyst. Effect of hydrogen spillover. Industrial & engineering chemistry research, 34(4), 1074-1080.

-10.0 wt%MoO_3 was applied since, in literature, this amount led to the highest Brønsted acid to metal-like sites ratio, resulting in the best hydroconversion of alkane.

References:

[1] Oloye, F. F., & Ololade, I. A. (2018). Influence of molybdenum loadings on the properties of MoO_3/zirconia catalysts. Chemistry Africa, 1(3-4), 119-126.

[2] Triwahyono, S., Jalil, A. A., Azman, H. A., & Mamat, C. R. (2015). Isomerization of C5-C7 Linear Alkanes over WO3-ZRO2 under Helium Atmosphere. Jurnal Teknologi, 75(6).

[3] Chen, J., Duan, Z., Song, Z., Zhu, L., Zhou, Y., Xiang, Y., & Xia, D. (2017). Relationship between surface property and catalytic application of amorphous NiP/Hβ catalyst for n-hexane isomerization. Applied Surface Science, 425, 448-460.

Comment 7:

It is better to make the XRD shape clearer and bigger and show the Miller indices on the peaks.

Author reply:

Thank you for the comment. As requested, the XRD patterns in Fig. 1 have been redrawn and included with the Miller indices on the peaks.

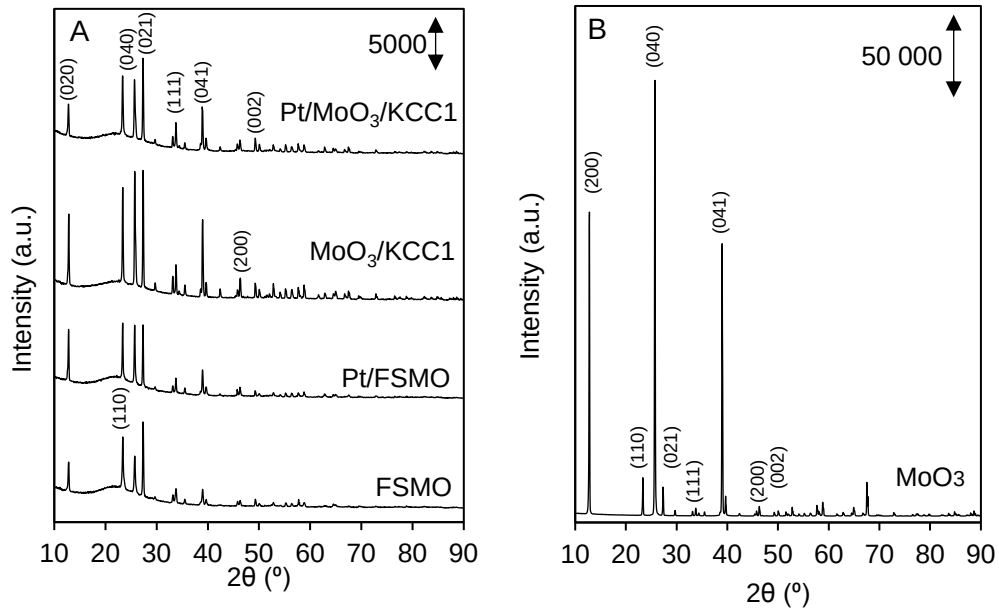

Fig. 1 XRD diffractogram for (A) MoO_3-based catalysts and (B) commercial MoO_3

Comment 8:

To express the stability of the catalysts against coke, the TGA spectra of these catalysts must be expressed.

Author reply:

Thank you for the comment. As requested, the authors have already added the temperature-programmed oxidation analysis to determine the coke content on the surface after 28 hours of testing Pt-FSMO and Pt/MoO3/KCC-1 samples, as highlighted in the revised manuscript.

Temperature-programmed oxidation (TPO) was carried out in Mettler Toledo TGA/SDTA/851e Thermo-gravimetric unit to estimate the carbonaceous deposition on the surface of spent catalysts within the temperature of 10-900 °C. Lines-154-156

The temperature-programmed oxidation analysis was conducted to quantify the extent of carbonaceous deposition on the spent catalysts. As depicted in Fig. S1, it was evidenced that Pt/FSMO possessed an inferior amount of coke compared to Pt/MoO_3/KCC-1, further proving the stability of isomerization activity within 28 h reaction. Lines 347-350

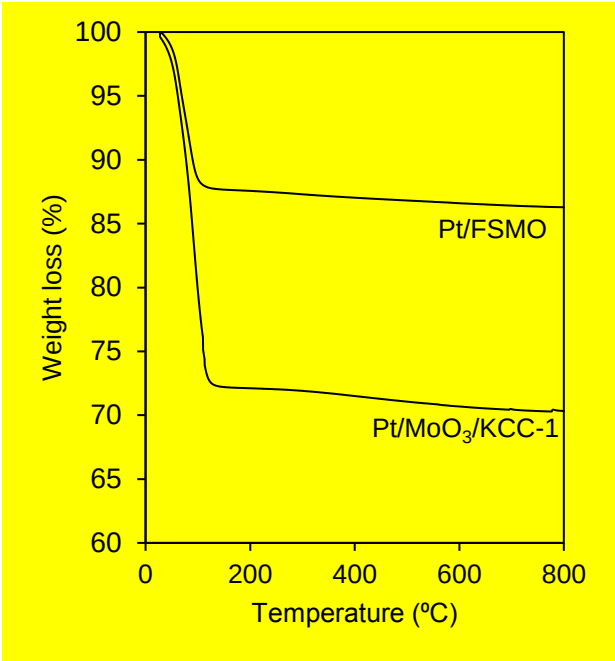

Fig. S1 TPO profile of spent Pt/FSMO and Pt/MoO_3/KCC-1 after catalyst stability test under 28 h time-on-stream at 250 ºC

HIGHLIGHTS

- FSMO, MoO_3/KCC-1, Pt/FSMO, and Pt/MoO_3/KCC-1 was synthesized for C_7 isomerization
- Mo insertion in Si-matrix induced Si-O-Mo formation, intensifying Lewis acid sites
- Pt inclusion promoted H_2 dissociation and enriched the amount of Lewis acid sites
- The highest *i*-C_7 yield of about 63.6% was attained for Pt/FSMO at 250 °C
- Excellent stability with low cracking revealed by Pt/FSMO compared to Pt/MoO_3/KCC-1

GRAPHICAL ABSTRACT

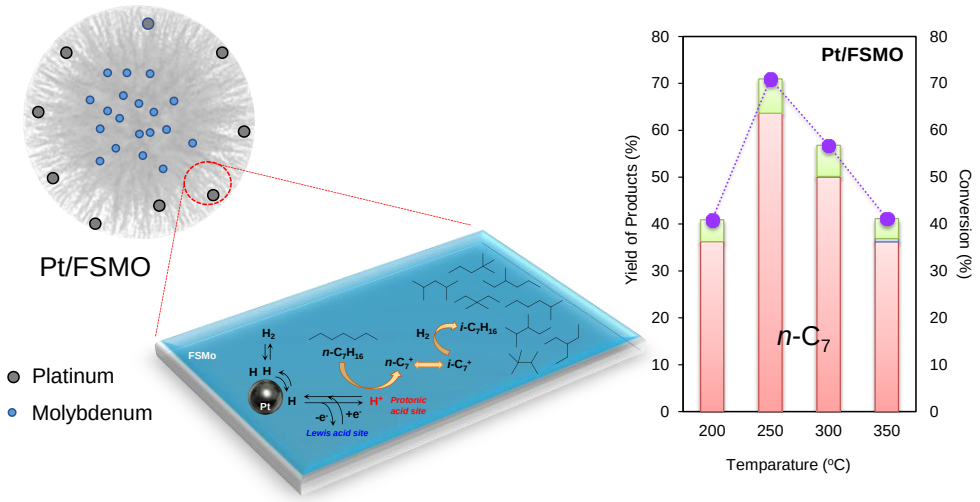

Mechanistic studies of lower temperature isomerization of n-heptane over fibrous silica molybdenum catalyst

M.B. Bahari[c], A.A. Jalil[a,b*], C.R. Mamat[c], N.S. Hassan[a,b], M.H. Razak[a], N.M. Izzudin[a], M.A.A. Aziz[a], N.F. Khusnun[b], M.A.H.Aziz[c], A.F.A. Rahman[b], W. Nabgan[d], Saravanan Rajendran[e]

[a] *Faculty of Chemical and Energy Engineering, Universiti Teknologi Malaysia, 81310 UTM Johor Bahru, Johor, Malaysia.*

[b] *Centre of Hydrogen Energy, Institute of Future Energy, Universiti Teknologi Malaysia, 81310 UTM Johor Bahru, Johor, Malaysia.*

[c] *Faculty of Science, Universiti Teknologi Malaysia, 81310 UTM Johor Bahru, Johor, Malaysia.*

[d] *Departament d'Enginyeria Química, Universitat Rovira i Virgili, Av Països Catalans 26, 43007, Tarragona, Spain*

[e] *Departamento de Ingeniería Mec´anica, Facultad de Ingeniería, Universidad de Tarapac´a, Avda. General Vel´asquez 1775, Arica, Chile*

**To whom correspondence should be addressed,*

Aishah Abdul Jalil (Ph.D.)

Tel: 60-7-5535581 Fax: 60-7-5536165

Email: aishahaj@utm.my

Abstract

Platinum (Pt) inclusion on fibrous silica molybdenum (FSMO) and MoO_3/KCC-1 catalysts has been prepared and utilized for the lower temperature (200-350 ºC) catalytic isomerization of n-heptane. The impact of Pt inclusion towards the structure, morphology, and acid distribution of catalysts was characterized by XRD, FTIR, N_2-physisorption, Py-IR, and H_2-IR. Compared with MoO_3/KCC-1, FSMO demonstrated superior MoO_3 dispersion and amount of Lewis acid site associated with the in-situ synthesis technique. Although Pt inclusion slightly lessened acid sites due to inevitable partial coverage by the Pt cluster, the considerably higher amount of Lewis acid sites compared to Brønsted and conjugated sufficiently for generating protonic acid sites for enriching the isomerization activity. In contrast to Pt/MoO_3/KCC-1 and undoped catalysts, Pt/FSMO achieved a superior conversion of 70.9% with 63.6% isomer yield at a low temperature of 250 ºC. The 28-h stability tests demonstrated that Pt/FSMO recorded stable isomerization activity, with a superior isomer yield (~48-52%) and inferior cracking yield (<3.0%) than Pt/MoO_3/KCC-1.

Keywords: n-C_7 isomerization; MoO_3-based catalysts; Platinum; Lewis acid; Protonic acid side

1.0 Introduction

Globally, comprehensive research and development initiatives have been undertaken to produce clean gasoline with low aromatics, olefins, sulphur, and high-octane numbers, in response to growing concerns over energy and environmental issues [1]. As a result, n-alkane isomerization has gained popularity as a safe and environmentally friendly method for enhancing gasoline quality [2]. This pathway allows n-alkanes with a linear carbon chain to be converted into branched isomers with a high research octane number (RON) [3, 4]. So far, tremendous effort has been put forth in researching light alkane isomerization since this compound processing has been industrialised. Yet, this technique has not been utilized for *n*-heptane and heavier alkanes due to the higher tendency of excessive development of cracking products as the conversion rate increases, leading to the deactivation of the catalyst due to the accumulation of coke on the surface's catalysts [5]. Hence, considering potential implementation, it is critical to look for relatively efficient and selective catalysts for heavy n-heptane isomerization while concurrently limiting cracking activities.

Bifunctional heterogeneous catalyst materials consisting of acidic supporting materials as well as hydrogenation/hydrogenation metal sites are among the popular catalysts used for the catalytic acid reaction [6, 7]. Both metallic and acidic functions influence the catalyst's properties and facilitate the alkane hydro-conversion. For instance, metal sites could generate carbonium ions via alkane dehydrogenation, a crucial intermediate species for initiating isomerization and cracking [8]. Once the acidity of the catalyst is mild, and the dehydrogenation activity of metal is substantial, a high yield of isomers is generated. In addition, when the dehydrogenation activity is more significant, unsaturated products are more hydrogenated, thus, inhibiting the escape acid-catalyzed skeleton rearrangement and cracking [9]. Throughout the scientific literature, *n*-alkane isomerization has made considerable use of

catalysts such as noble metals supported on microporous and mesoporous materials. In fact, it was found that the hydrogen atom spillover mechanism used by bifunctional heterogeneous catalysts could strongly induce isomerization [10]. Numerous acid-catalyzed reactions using various types of catalysts, like Pt/MoO_3 [11-13], Pt/WO_3-ZrO_2 [14], MoO_3/MSN [15], and Zn/HZSM-5 [10], have been explored for their spillover mechanisms.

Recently, the potential of the MoO_3 type catalysts has been extensively explored for a wide range of catalytic processes like methanation, olefin metathesis, alcohols oxidation, and isomerization accredited to MoO_3's exceptional features, including excellent stability and regeneration performance [16]. In addition, MoO_3 possessed both Lewis and Bronsted acid sites, which is crucial for *n*-alkane isomerization and provides superior selectivity for heptane isomerization compared to conventional catalysts. Incorporating second material as active sites into bifunctional catalysts has aroused considerable attention in recent years owing to the positive effects on isomerization performance, isomer selectivity, as well as stability. Second Noble materials like Pd and Pt have been extensively studied, attributed to their hydrogen spillover capability, boosting the isomerization activity. Indeed, the combination between Pt and MoO_3 in a hydrogen atmosphere can generate several active species, including H_xMoO_3 and MoO_2, that are utilized for isomerization [11, 17]. Previous work has demonstrated that incorporating Pt and MoO_3 into diverse supporting materials effectively improved n-heptane isomerization performance [11, 13]. Regrettably, it should be noted that there is a paucity of literature focusing on the usage of catalysts at low operating temperature.

Creating support with a dendrimer fibrous structure has recently received much attention [18]. This strategy can produce an ideal support material possessing vast surface area, tuneable pore volume, conveniently reachable inner surface, as well as superior thermal stability [19-21]. In fact, this approach has resulted in a positive effect on the catalytic activity of all catalytic pathways, including isomerization [4], methanation [22], cumene cracking [23],

and dry reforming [24]. According to the researchers, the improvement was attributable to the enhanced accessibility of active areas within this particular shape. Inspired by the previous study, we synthesized fibrous silica-molybdenum trioxide (FSMO) supported platinum (Pt) and assessed their capability in *n*-heptane isomerization at low reaction temperature for the first time. The fibrous silica in the Pt/FSMO catalyst induces Si-O-Mo formation to enhance Lewis acid site quantity, which will cause a growth in protonic acid site generation, thus enriching *n*-heptane isomerization activity. The physicochemical features of the studied catalysts were analysed in detail via XRD, N_2 physisorption and several in-situ IR analysis. The isomerization pathway over Pt/FSMO catalyst is also elucidated.

2.0 Experimental

2.1 MoO_3-based catalysts synthesis

Fibrous silica-molybdenum (FSMO) and KCC-1 were prepared corresponding to the microemulsion approach as detailed in the literature [25, 26]. In brief, a homogeneous solution consisting of CTAB and urea was acquired by mixing and stirring both chemicals in distilled water for 15 min (25ºC). Thereafter, butanol and toluene were poured into the mixture under continuous agitation at ambient temperature before being dopped with the specified amount of MoO_3 seed. The resulting mixture was further agitated at ambient temperature for two hours to guarantee TEOS was hydrolyzed entirely prior to the six-hour hydrothermal treatment in microwave irradiation (120 ºC, 400 W). Afterwards, the acquired solution was air-dried in an oven (24 h, 110 ºC) to eradicate the moisture before furnace-calcination (6 h, 550 ºC) to gain desired FSMO. On the contrary, for KCC-1 support production, TEOS was dropped along with

butanol and toluene before being treated with a similar condition for hydrothermal treatment, air-drying, and furnace-calcination.

The incipient wetness impregnation technique, as reported by Siang et al. [27], was applied in this work to generate Pt/FSMO and MoO_3/KCC-1 catalysts. For KCC-1 supported 10.0 wt%MoO_3 catalyst, a calculated amount of ammonium heptamolybdate ($[NH_4]_6Mo_7O_{24}$) as the metal precursor and KCC-1 support were separately dissolved in the deionized water prior to the impregnation step. After both solutions were mixed and agitated at ambient temperature for four hours, the resulting mixture was further air-dried in an oven (24 h, 110 ºC) and subsequently underwent furnace-calcination (6 h, 550 ºC), which yielded MoO_3/KCC-1. A similar approach as those stated earlier was employed to prepare Pt/FSMO using chloroplatinic acid hexahydrate ($H_2PtCl_6 \cdot 6H_2O$) as the metal precursor (0.1 wt%Pt) over FSMO support. For Pt/MoO_3/KCC-1 catalyst preparation, the sequential incipient wetness impregnation technique was employed by discretely dissolved $H_2PtCl_6 \cdot 6H_2O$ and as-synthesized MoO_3/KCC-1 in deionized water. Afterwards, both dissolved materials were combined, agitated, dried, and calcined, similar to those earlier impregnation steps to acquire Pt/MoO_3/KCC-1.

2.3 Characterizations of MoO_3-based catalysts

The crystalline structure of studied catalysts was assessed by X-ray diffractogram (2θ = 20-85°, step size = 0.02) on a Bruker Advance D8 diffractometer equipped with Cu Ka radiation (λ =0.154 nm, V = 40 kV, I = 40m A). The Barrett-Joyner-Halenda (BJH) and Brunauer-Emmet-Teller (BET) techniques were applied to measure the catalyst's surface area and pore properties using liquid nitrogen at -196 °C in a Beckman Coulter SA3100 unit. The one-hour-outgassed treatment was initially employed at 300 °C prior to the nitrogen adsorption

at 77 K for eradicating the moisture and contaminants. The functional groups of the studied catalysts were appraised via the FTIR-KBr approach at the range of 1600-400 cm^{-1} with 5 cm^{-1} resolutions on the FT-IR spectrometer unit (Agilent Cary 660). The acidity of studied catalysts was scrutinized through Py-IR adsorption on stainless-steel cells with two CaF2 windows sealed. Initially, the tested catalysts were pelletized before exposing them to 4 Torr of pyridine stream for a quarter-hour at 150 °C. Afterwards, the desorption of pyridine from tested catalysts was carried out at a different temperature within 150-350°C. H_2-IR adsorption was also operated in similar equipment for Py-IR adsorption. After activation treatment, the tested catalysts were cooled to room temperature before being subjected to 20 Torr of the hydrogen stream under rising temperature up to 350 °C. Temperature-programmed oxidation (TPO) was carried out in Mettler Toledo TGA/SDTA/851e Thermo-gravimetric unit to estimate the carbonaceous deposition on the surface of spent catalysts within the temperature of 10-900 °C.

2.4 n-C_7 Isomerization evaluation

The micro-catalytic pulse reactor was utilized to evaluate *n*-heptane isomerization within 200-350 °C. About 0.2 g of the studied catalyst was employed in the reactor, followed by exposure to the 100 ml min^{-1} of O_2 stream (1 h, 400 °C) and then 100 ml min^{-1} H_2 stream (3 h, 400 °C) as the pre-treatment step. Subsequently, the tested catalyst was cold down in a similar H_2 stream to reach 150 °C. After stabilizing and reaching the necessary conditions, about two µmol of n-C_7 was driven into the reactor filled with an H_2 stream (100 ml min^{-1}) to commence the isomerization process. An online gas chromatograph (Agilent 6090N, FID, HP-5), connected with a utilized micro-catalytic pulse reactor, scrutinized the isomerization product. The isomerization product was confined using N_2 (-196 °C) before being flash-evaporated into

the gas chromatograph system. The isomerization activity was estimated based on the conversion (X), yield (Y), and selectivity (S), as expressed in Eqs. (1)-(3).

$$X_i(\%) = \frac{\sum A_i - A_{r,i}}{\sum A_i} \times 100\% \quad (1)$$

$$S_i(\%) = \frac{A_i}{\sum A_i - A_{r,i}} \times 100\% \quad (2)$$

$$Y_i = \frac{X_i \times S_i}{100} \quad (3)$$

Where A_i = corrected chromatographic area for a specific product and $A_{r,i}$ = corrected chromatographic area for residual of n-heptane species, in weight percent unit.

3.0 Results and Discussion

3.1 Characterization analysis

XRD diffractograms for commercial MoO_3 and generated catalysts are shown in Figs. 1A-B. All of the prepared catalysts showed a clear peak at 2θ = 10°-70° on the plot. The XRD pattern of the MoO_3 catalyst demonstrated that it possesses an orthorhombic structure consistent with standard data (JCPDS Card No: 050508) [28]. The crystallite peaks corresponded to the MoO_3 witnessed at an angle of 2θ about 12.9° (020), 23.4° (110), 25.8° (040), 27.4° (021), 33.7° (111), 39.0° (041), 46.1° (200), and 49.4° (002) in FSMO and MoO_3/KCC-1 [29]. The inferior intensity of crystallite peaks of FSMO than MoO_3/KCC-1 catalyst, indicating that the in-situ synthesis strategy for generating FSMO promoted the well-distribution of Mo on the Si framework in comparison to MoO_3/KCC-1 prepared via the incipient wetness impregnation approach [30]. Furthermore, due to the small size of the Pt

192 species dispersed on the FSMO and MoO_3/KCC-1, possibly below than XRD detection limit,
193 further explained for no visible diffraction peaks assignable to Pt species over Pt/FSMO and
194 Pt/ MoO_3/KCC-1 [31].

195 The FTIR spectra (1400-400 cm^{-1}) of the functional groups owned by studied catalysts
196 are depicted in Fig. 2. Evidently, all the studied catalysts displayed five identical IR bands
197 ranging from 1095 cm^{-1} to 467 cm^{-1}. The absorption peaks appeared at a wavenumber of 1095
198 cm^{-1}, 956 cm^{-1}, 802 cm^{-1}, and 467 cm^{-1} are linked to the vibration of asymmetric Si-O-Si,
199 external Si-OH, symmetric Si-O-Si, and bending Si-O-Si, respectively [32]. Meanwhile,
200 absorption peaks identified at a wavenumber of 902 cm^{-1} overall studied catalysts signified
201 weak Mo=O vibration [33, 34]. Following the modification of MoO_3 into FSMO, a drop in the
202 intensity for the IR band at 956 cm^{-1} (external Si-OH vibration) for FSMO compared to
203 MoO_3/KCC-1 suggesting that more replacement of hydrogen atom by Mo ions to form Si-O-
204 Mo, associated with the alternately aligned SiO_2 and MoO_3 in the fibrous structure. As a
205 consequence, this improvement could strengthen the interaction of MoO_3-SiO_2. This
206 observation was also reported by Sawal et al. [35] and Hitam et al. [36]. Remarkably, the FTIR
207 spectrum of FSMO was almost identical to that of Pt/FSMO, revealing no significant changes
208 towards the silicate framework of FSMO after Pt incorporation. Apart from that, it is apparent
209 from these FTIR spectra that most of the IR bands for FSMO and MoO_3/KCC-1 catalysts
210 experienced a slight decrease in intensity compared to Pt-loaded catalysts, indicating the
211 successful impregnation of Pt over the tested catalysts, creating new interaction between Pt and
212 SiO_2.

213 Further investigation was performed using N_2 physisorption analysis to examine
214 synthesized catalysts' textural properties; the results are presented in Fig. 3. As can be observed,
215 all the prepared catalysts demonstrated a type IV isotherm profile with a typical H3 hysteresis
216 loop, confirming the mesoporous structure characteristic of the synthesized catalysts (Fig. 3A)

[30]. In addition, in the absence of Pt element, both FSMO and MoO_3/KCC-1 catalysts exhibited comparable N_2 uptakes. However, when Pt was loaded onto the catalyst surface, the N_2 uptakes for Pt/MoO_3/KCC-1 increased substantially at higher relative pressure, while Pt/FSMO catalyst demonstrated an insignificant change. This result may be explained by the fact that high interaction between the Pt element and MoO_3 of Pt/MoO_3/KCC-1 reduced the pore blockage of the MoO_3 on the mesopore of the KCC-1 [36]. Besides, the total pore volume for MoO_3/KCC-1 catalyst increased after adding Pt (Table 1), which indirectly supported the earlier statement. Meanwhile, for Pt/FSMO catalyst, the pore volume was slightly decreased compared to the FSMO catalyst, suggesting the filling of Pt inside the FSMO mesopore [30].

Barrett-Joyner- Halenda (BJH) approach was applied to assess the average pore diameter, as shown in Fig. 3B. The BJH pore size distribution demonstrated the pore diameter of the synthesized catalysts placed within 3-40 (Å), showing the intrinsic of mesopores features. It is worth noting that the pore distribution of FSMO and KCC-1-supported MoO_3 catalysts were considerably grown by adding Pt, probably due to the high mesoporous of Pt that created inter-dendrimer distances [37]. For a better understanding of the textural properties of as-prepared catalysts, the results were tabulated and presented in Table 1. As noticed, the surface area for both FSMO (114.6 m^2/g) and MoO_3/KCC-1 (221.3 m^2/g) was reduced considerably after adding Pt, suggesting that pores of FSMO and MoO_3/KCC-1 catalysts were partially blocked by Pt particles [38]. This trend further inferred that the alteration of catalyst structure could lead to surface area changes.

The efficacy of the isomerization reaction was considerably linked to the number and intensity of the surface acidity in catalysts. Thus, Py-IR measurement was applied to assess the distribution of Lewis and Brønsted acidic sites over activated catalysts at different temperatures (150-250 ºC), and the Py-IR spectra are illustrated in Fig. 4. As can be seen, all of the studied catalysts disclosed three IR bands ranging within 1570-1420 cm^{-1}. It was noted that IR bands

spotted at 1454 cm^{-1} and 1539 cm^{-1} belonged to pyridinium ions adsorption on Lewis and Brønsted acid sites, respectively [39, 40]. In addition, the appearance of IR band at a wavenumber of 1488 cm^{-1} over all tested catalysts related to Brønsted and Lewis acid sites combination [41, 42]. Interestingly, by comparing FSMO and MoO_3/KCC-1, it was noticed that Lewis acid sites intensity for FSMO was considerably higher than KCC-1 supported MoO_3 catalysts, possibly ascribed to the more replacement of -H (from Brønsted) by Mo ions in forming Si-O-Mo (Lewis acid sites), resulted from the fibrous framework, in line with FTIR finding. The decline in Lewis and Brønsted acid site intensity was witnessed after Pt was impregnated onto FSMO and MoO_3/KCC-1, suggesting the inevitable partial coverage of acidic sites by the Pt cluster. A comparable phenomenon was claimed by Setiabudi et al. [43] and Teh et al. [5] during the isomerization over Ir/Pt-HZSM5 and Pt/MoO_3-HBEA catalysts, respectively.

The impact of outgassed temperature (150-350 ºC) towards the distribution of acidic sites on studied catalysts is also elucidated in Fig. 4. The pyridine molecules adsorbed on weak acid sites typically desorbed at a lower temperature whilst higher outgassing temperature is required for desorbing pyridine molecules for strong acid sites. All tested catalysts appeared to demonstrate intense interaction between pyridine and acidic sites at 150 ºC and remained firm at the outgassing temperature of 150 ºC. The considerable decline in the intensity of acidic sites for all studied catalysts was evidenced along with the rising outgassing temperature of up to 350 ºC, signifying that weak-to-moderate Brønsted and Lewis acid sites are dominantly located on those catalysts. This outcome also accords with the trends observed by other studies by Fatah et al. [15] and Ma et al. [44] during the Py-IR evaluation over Pt/MSN, MoO_3/MSN, and Al/SBA catalysts, respectively. Previous studies on isomerization have noted that the more significant amount and intensity of acid sites of catalysts favour cracking instead of

isomerization reaction [5, 45]. Thus, the optimum amount with moderate acid sites is preferable for enhanced isomerization.

Fig.5 disclosed the Py-IR spectra in 1600-1400 cm^{-1} when the pyridine pre-adsorbed catalysts were heated in H_2 gas at elevated temperatures. The heating of all catalysts under H_2 gas exposure modified the intensity of Lewis and Bronsted acid sites at 1446 cm^{-1} and 1538 cm^{-1}, respectively. Particularly, the intensity of Lewis acid sites declined with the simultaneous rise in the Bronsted acid sites, indicating the formation of protonic acid sites from hydrogen atoms spillover [4]. In general, protonic acid sites formed through interconversion of the Lewis acid sites. In this study, the protonic acid site formation rate is higher in all catalysts at lower temperatures (250-300 °C), as presented in Fig. 6. For FSMO and MoO_3/KCC-1, the formation of protonic acid sites was probably due to the interaction of the Mo atom with the proton in the form (MoO_x)-$(H_y)^+$) that generated from releasing of the electron by atomic hydrogen, as similarly reported by previous studies [15]. Interestingly, adding Pt into both catalysts significantly increased the protonic acid site formation rate, especially at low operating temperatures. These results indicated that Pt heightened the interaction of the hydrogen atom with the surface of FSMO and MoO_3/KCC-1. This phenomenon has also been observed in Pt/WO_3-ZrO_2 catalysts by Triwahyono et al. [46].

3.2 n-C_7 Isomerization performance

Fig. 7 depicts the isomerization activity of FSMO, MoO_3/KCC-1, Pt/FSMO, and Pt/MoO_3/KCC-1 in *n*-heptane isomerization within 200-350 ºC. Notably, all catalysts suffered a decrement in the yield of isomers along with the rise in operating temperature, which attained optimum yield at 200-250 ºC and decreased above 250 ºC. This trend was associated with the domination of cracking reaction compared to heptane isomerization at a higher temperature. It

is interesting to note that FSMO presented a superior *n*-heptane conversion (53-55%) and yield of isomers (46-52%) compared to MoO_3/KCC-1, regardless of reaction temperature owing to the considerably greater average pore size of FSMO (19.8 nm > 12.4 nm), as provided in Table 1. The enlargement in pore size was believed to minimize the transport restriction throughout the catalysts as well as improve the diffusion steps [47, 48]. Additionally, the high isomerization activity of FSMO than MoO_3/KCC-1 was probably related to possessing a moderate amount of weak Bronsted acid sites. This finding is accorded with the result from Py-IR with different outgassing temperatures (Fig. 4), which showed that FSMO possessed a lower amount of Bronsted acid sites than KCC-1 supported MoO_3 catalysts since there was more replacement of hydrogen atom (from Brønsted Si-OH) by Mo ions in forming Si-O-Mo (Lewis acid sites). Consequently, this domination facilitated the formation of the protonic acid site via H_2 dissociation and spillover, resulting in high isomerization activity. This trend was also evident from the experimental work of Triwahyono et al. [4], in which the modification of Y zeolite (HY) into fibrous silica@Y zeolite for C_5-C_7 isomerization.

Improvement in conversion and yield of isomer was noticed, especially at a lower temperature (<350 ºC) after incorporating Pt over FSMO and MoO_3/KCC-1 (Fig. 7). The results demonstrated that Pt/FSMO achieved optimal conversion of 70.9% with 63.6% isomer yield at a temperature of 250 ºC. Instead, Pt/MoO_3/KCC-1 recorded a maximum conversion of 61.7% with the yield of an isomer of 56.5% at 200 ºC. The enhancement in the isomerization activity after Pt addition, especially at low temperatures, was plausibly attributed to the considerably higher amount of Lewis acid sites than Brønsted and conjugated acid sites as demonstrated in Py-IR (cf. Fig. 4), appropriately sufficient in generating protonic acid sites for enriching the isomerization activity. Furthermore, this improvement could be linked to new active site species generated from the interaction of Pt-support lattice defects [5]. Thus, the addition of Pt over FSMO and MoO_3/KCC-1 could facilitate the activation of hydrogen

molecules via dissociation, enhancing the spillover process and thus enriching the formation of protonic acid sides and hydrides for generating more isomer products. Interestingly, the yield of cracking exhibited by Pt/FSMO is slightly lower compared to FSMO at 350 ºC, suggesting that Pt doped over FSMO effectively suppressed the binding interaction between FSMO and atomic hydrogen, thus enriching the formation of hydride ions that are responsible for the generation of the desired isomerization products [17]. In contrast, the high yield of cracking witnessed at 350 ºC for Pt/MoO_3/KCC-1 probably indicates that Pt incorporation could not restrain the binding interaction between support and spillover hydrogen atom, thus lowering the hydride generation. At low hydride availability, the hydrogen atoms' migration will occur slowly compared to the β-fission, favouring more cracking products than isomers [49].

Increased isomerization activity with the incorporation of Pt is also consistent with those of Al-Kandari et al. [50], who have evaluated the catalyst's isomerization activity over TiO_2-supported MoO_3. They found that Pt incorporation effectively improved the bifunctional metallic-acidic system of the MoO_3/TiO_2 catalyst, causing an improvement in *n*-heptane isomerization activity at 573 K. In different work, Matsuda and coworkers [51] highlighted that n-heptane isomerisation could be enhanced by introducing Pt over the reduced MoO_3 catalysts. The authors noticed that this effort could produce acidic molybdenum oxyhydride (MoO_xH_y), a crucial active site for enhancing the isomerization performance. Teh et al. [5] also discovered a significant improvement in n-heptane isomerization after incorporating Pt on the MoO_3-HBEA catalyst, accredited to the role of Pt in dissociating hydrogen molecule, suppressing the MoO_3-spillover hydrogen atom interaction, while enriched protonic acid sites quantity.

The stability performance of Pt/FSMO and Pt/MoO_3/KCC-1 in *n*-heptane isomerization under 28 h time-on-stream with intervals of 15 min for each dose was plotted in Fig. 8. Although Pt/MoO_3/KCC-1 recorded superior conversion (>~60.0%) as compared to Pt/FSMO, this catalyst experienced unsteady isomerization activity within 28 h reaction. This

phenomenon probably resulted from the high cracking side reaction, which could deactivate the catalysts as a consequence of high coke accumulation. On the contrary, Pt/FSMO recorded stable isomerization activity, especially with a better isomer yield (~48-52%) and a lower cracking yield (<3.0%). The temperature-programmed oxidation analysis was conducted to quantify the extent of carbonaceous deposition on the spent catalysts. As depicted in Fig. S1, it was evidenced that Pt/FSMO possessed an inferior amount of coke compared to Pt/MoO_3/KCC-1, further proving the stability of isomerization activity within 28 h reaction. This trend proves the efficient role of Pt in enhancing the Lewis acid site of the catalyst for generating essential protonic acid, minimizing the strong support-spillover hydrogen atom interaction, and assisting in lessening the coke accumulation via hydrogenation. Thus, it is noteworthy that Pt/FSMO catalysts have excellent potential for long-term isomerization reactions.

3.4 Proposed reaction pathway

Based on the characterizations and *n*-heptane isomerization test, as mentioned before, it can be evidenced that MoO_3 modification into the fibrous structure of support with silica (FSMO), along with the incorporation of Pt element, could enrich the generation of Lewis acid sites, thus, aiding in essential protonic acid sites generation at low temperature. This factor further explains the excellent performance of Pt/FSMO catalyst on *n*-heptane isomerization at a lower temperature. In order to comprehend the isomerization mechanism, the proposed reaction pathway for *n*-heptane isomerization over Pt/FSMO is clarified in Fig. 9.

At the initial pathway, the pre-treatment of Pt/FSMO in the H_2 stream resulted in the instigation of Pt-oxide into metallic Pt, the crucial hydrogen activation sites. The H_2 molecules adsorbed on metallic Pt were further dissociated into two species of hydrogen atoms. This

dissociation step is crucial in isomerization since it contributes to acid site generation, favouring the isomer generation instead of the cracking and polymerization of *n*-C_7 via ß-scission [4, 52]. After splitting, the produced hydrogen atom was spilt over onto the acidic surface of FSMO and further diffused towards the Lewis acid sites. The spilt over of hydrogen atoms then transferred an electron towards Lewis acid sites and bonded with Brønsted sites of FSMO for forming protonic acid site (B-H^+ species). The generated protonic acid sites then transferred protons to *n*-heptane, resulting in the formation of heptyl carbenium ion (*n*-C_7^+) species. Afterwards, the accepted proton in the carbenium ion was moved along the hydrocarbon chain, forming the iso-heptyl carbenium ion (*i*-C_7^+) species. Simultaneously, the electron confined by the Lewis acid sites was further reacted with another split hydrogen atom to become a hydride ion and attached to the Lewis acid site (L-H^-). Then, the produced L-H^- species further interacted with *i*-C_7^+ species contributing to the generation of the desired isomerization products. This proposed mechanism further proved that isomerization yield was strongly influenced by the protonic acid sites and hydrate ions created from H_2 dissociation in the presence of Pt. However, according to Hattori et al. [49], if there were excessive hydride species during the reaction, the concentration of carbenium ions would considerably drop, lowering the isomerization activity.

3.5 Comparative analysis

In order to evaluate the competency of our generated MoO_3-based catalysts, a comparative analysis (cf. Table 2) towards the reported MoO_3-based catalyst's activity over *n*-heptane isomerization was conducted. Fatah et al. [15] compared the isomerization activity of over MoO_3- and Pt- supported with MSN in the system consisting of H_2 or N_2 as the carrier. The high performance of MoO_3-supported with MSN conducted in the H_2 system was recorded

with mono- and di-branched iso-heptane, which yielded about 81.3 and 12.4%, respectively, resulting from $(MoO_x)^-(H_y)^+$ active sites formation. On the other hand, the authors claimed that the incompetence of the Pt- supported with MSN to generate protonic acid sites led to poor isomerization activity. The author also evaluated the isomerization performance over MoO_3 supported by KCC-1, incorporating the phosphorous element [16]. The generation of $(MoO_x)^-(H_y)^+$ active site along with the involvement of acidic centres from phosphorus inclusion and MoO_3, caused the improvement in the rate of n-heptane conversion.

In another effort, Ruslan et al. [53] investigated the role of the acid site of MoO_3-ZrO_2 catalysts toward n-heptane isomerization activity. Notably, the existence of the ZrO_2 tetragonal phase in the catalysts contributed to enhancement in the number of Lewis acid sites, easing active protonic acid site generation, thus responsible for the improvement of isomerization activity and stability. Nevertheless, the authors witness superior cracking activity compared to isomerization, which gradually increases with rising temperature from 300-400 ^oC. Besides, Matsuda et al. [51] emphasized the acid site's role and its impact on isomerization performance over Pt/MoO_3-SiO_2. They concluded that the isomerization selectivity of Pt/MoO_3-SiO_2 was enhanced from 88.7-97.8% by raising the amount of MoO_3 employed from 20-100wt%, related to the growth in the number of acid sites. Meanwhile, the cracking selectivity of Pt/MoO_3-SiO_2 was significantly reduced from 10.7% to 1.9% with the rising MoO_3 loading.

Liu et al. [54] stated that HBEA zeolite-supported molybdenum phosphide (MoP) demonstrated superior isomerization selectivity (67.8%) compared to tungsten phosphide supported on Hβ (50.1%) and HMCM22 (64.2%). The authors also proposed that doping Ce, Ni, and Cr elements over MoP/Hβ substantially enriched the activity with Cr-promoted catalyst promoted the superior isomerization selectivity around 73.1%, owing to the increment in the density of strong acid sites of MoP/Hβ. Works by Sakagami et al. [11] and Parsafard et al. [55] revealed a positive impact towards isomerization activity over MoO_3 and ZrO_2-HMS catalysts,

respectively, accredited to the presence of Pt, which enhances protonic acid site generation via H_2 dissociation and spillover phenomenon. This trend is in accordance with our findings. However, the negative impact of Pt incorporation was experienced by Triwahyono et al. [46] over MoO_3-ZrO_2. The authors justified that although Pt addition improved the hydrogen adsorption rate, Pt addition has caused the intensification of Lewis acid sites instead of forming more active protonic aicd sides, consequently lowering the isomerization activity.

Table 2 shows that our generated catalysts exhibited better or comparably to other MoO_3-based catalysts utilized for the isomerization of n-heptane, especially in conversion and isomerization selectivity. Indeed, the inferior cracking selectivity of studied catalysts compared to the literature indicates that all generated catalysts are favoured to isomerization activity compared to cracking. The outstanding performance of these generated catalysts, despite the absence of Pt, is ascribed to the fibrous silica morphology, which contributes to the formation of more Si-O-Mo for enriching Lewis acid sites quantity, causing growth in protonic acid sites generation, hence, enhancing the isomerization activity. Moreover, after Pt was doped, the enhancement of the Lewis acid site of the catalyst for generating essential protonic acid was evidenced, assisting in suppressing the strong support-spillover hydrogen atom interaction and lowering the coke accumulation. Thus, isomerization activity improved, especially at the lower reaction temperature.

4.0 Conclusion

This study appraised and compared the impact of Pt inclusion on physiochemical characteristics and isomerization activity of synthesized MoO3-based catalysts (FSMO and MoO3/KCC-1). XRD results indicated that the in-situ synthesis strategy effectively improved

the distribution of Mo particles in the Si framework than via incipient wetness impregnation. Additionally, the in-situ synthesis strategy promotes Si-O-Mo formation, associated with the alternately aligned SiO_2 and MoO_3 in the fibrous structure, strengthening MoO_3-SiO_2 interaction, as proved in FTIR analysis. Consequently, Py-IR analysis revealed that Lewis acid sites intensity for FSMO was considerably higher than KCC-1 supported MoO_3 catalyst, ascribed to the more replacement of -H (from Brønsted) by Mo ions in forming Si-O-Mo (Lewis acid sites). Nevertheless, it is noteworthy that Pt inclusion over FSMO and MoO_3/KCC-1 lessened those acid sites owing to the inevitable partial coverage by the Pt cluster.

The isomerization tests revealed enlargement in pore size, and the possession of a moderate amount of weak Bronsted acid sites contributed to the superior n-heptane conversion (53-55%) and yield of isomers (46-52%) for FSMO compared to MoO_3/KCC-1, regardless of reaction temperature. Meanwhile, incorporating Pt over FSMO and MoO_3/KCC-1 improved the conversion and yield of isomer, especially at a lower temperature (<350 ºC), by achieving optimal conversion of 70.9% with 63.6% isomer yield at a temperature of 250 ºC. At the same time, Pt/MoO_3/KCC-1 recorded a maximum conversion of 61.7% with the yield of an isomer of 56.5% at 200 ºC. This trend was plausibly accredited to the considerably more significant amount of Lewis than Brønsted and conjugated acid sites, sufficient to generate protonic acid sites for enriching the isomerization activity. Pt/FSMO recorded stable isomerization activity within 28 h, with a better isomer yield and a lower cracking yield than Pt/MoO_3/KCC-1 due to the efficient role of Pt in lessening the coke accumulation via hydrogenation. The findings of this study demonstrated the potential of Pt/FSMO as the catalyst for isomerization reactions.

Conflict of Interest

The authors hereby declare no conflict of interest for the research work reported in this manuscript.

Authorship contribution

M.B. Bahari: Project administration, Visualization, Writing - Original Draft, Methodology, **A.A. Jalil:** Project administration, Funding acquisition, Conceptualization, Visualization, Supervision, **N.S. Hassan:** Visualization, Writing - Original Draft, **MH Razak:** Investigation**,** Formal analysis, **N.M. Izzudin:** Investigation**,** Formal analysis, **NF. Khusnun:** Visualization, Writing - Original Draft**, M.A.H. Aziz**: Investigation**,** Formal analysis, **A.F.A. Rahman:** Investigation**,** Formal analysis, **W. Nabgan:** Investigation**,** Formal analysis, **Saravanan Rajendran:** Investigation**,** Formal analysis,

Acknowledgement

We are grateful for the financial support from Universiti Teknologi Malaysia (UTM) for the UTM Fundamental Research (No.22H51) and Professional Development Research University grant (No. 05E72).

References

[1] Smolikov MD, Shkurenok VA, Bikmetova LI, Prosvirin IP, Gulyaeva TI, Bukhtiyarov AV, et al. Effect of hydrogen reduction and palladium promotion of tungstate-modified zirconia on isomerization of heptane. Molecular Catalysis. 2022;529:112527.

[2] Ali NS, Alismaeel ZT, Majdi HS, Salih HG, Abdulrahman MA, Saady NMC, et al. Modification of SBA-15 mesoporous silica as an active heterogeneous catalyst for the hydroisomerization and hydrocracking of n-heptane. Heliyon. 2022;8:e09737.
[3] Saginayev A, Dosmurzina E, Apendina A, Dossanova B, Imangaliyeva B. Development of individual approaches to the use of the gasoline fraction as a raw material for the process of hydrocatalytic isomerization. Materials Science for Energy Technologies. 2022.
[4] Triwahyono S, Jalil AA, Izan SM, Jamari NS, Fatah NAA. Isomerization of linear C5–C7 over Pt loaded on protonated fibrous silica@Y zeolite (Pt/HSi@Y). Journal of Energy Chemistry. 2019;37:163-71.
[5] Teh LP, Setiabudi HD, Sidik SM, Annuar NHR, Jalil AA. Synergic role of platinum (Pt) and molybdenum trioxide (MoO_3) promoted HBEA zeolite towards n-heptane isomerization. Materials Chemistry and Physics. 2021;263:124406.
[6] Ono Y. A survey of the mechanism in catalytic isomerization of alkanes. Catalysis Today. 2003;81:3-16.
[7] Samad JE, Blanchard J, Sayag C, Louis C, Regalbuto JR. The controlled synthesis of metal-acid bifunctional catalysts: The effect of metal: acid ratio and metal-acid proximity in Pt silica-alumina catalysts for n-heptane isomerization. Journal of Catalysis. 2016;342:203-12.
[8] Blomsma E, Martens J, Jacobs P. Isomerization and hydrocracking of heptane over bimetallic bifunctional PtPd/H-beta and PtPd/USY zeolite catalysts. Journal of Catalysis. 1997;165:241-8.
[9] Sabyrov K, Musselwhite N, Melaet G, Somorjai GA. Hydroisomerization of n-hexadecane: remarkable selectivity of mesoporous silica post-synthetically modified with aluminum. Catalysis Science & Technology. 2017;7:1756-65.
[10] Triwahyono S, Jalil AA, Mukti RR, Musthofa M, Razali NAM, Aziz MAA. Hydrogen spillover behavior of Zn/HZSM-5 showing catalytically active protonic acid sites in the isomerization of n-pentane. Applied Catalysis A: General. 2011;407:91-9.
[11] Sakagami H, Ohno T, Takahashi N, Matsuda T. The effects of Na loading on catalytic properties of H_2-reduced Pt/MoO_3 for heptane isomerization. Journal of Catalysis. 2006;241:296-303.
[12] Triwahyono S, Jalil AA, Timmiati SN, Ruslan NN, Hattori H. Kinetics study of hydrogen adsorption over Pt/MoO_3. Applied Catalysis A: General. 2010;372:103-7.
[13] Matsuda T, Sakagami H, Takahashi N. H_2-reduced Pt/MoO_3 as a selective catalyst for heptane isomerization. Catalysis Today. 2003;81:31-42.
[14] Cheng TX, Kabashima H, Hattori H. Effects of hydrogen and hydrogen sulfide on cumene cracking catalyzed by Pt/WO_3-ZrO_2. Control of acidic and metallic functions. Reaction Kinetics and Catalysis Letters. 2000;69:201-7.
[15] Fatah NAA, Triwahyono S, Jalil AA, Ahmad A, Abdullah TAT. n-Heptane isomerization over mesostructured silica nanoparticles (MSN): Dissociative-adsorption of molecular hydrogen on Pt and Mo sites. Applied Catalysis A: General. 2016;516:135-43.
[16] Fatah NAA, Triwahyono S, Jalil AA, Salamun N, Mamat CR, Majid ZA. n-Heptane isomerization over molybdenum supported on bicontinuous concentric lamellar silica KCC-1: Influence of phosphorus and optimization using response surface methodology (RSM). Chemical Engineering Journal. 2017;314:650-9.
[17] Matsuda T, Uchijima F, Sakagami H, Takahashi N. H_2-reduction of Pt/MoO_3 to MoO_x with a large surface area and its catalytic activities for the conversions of heptane and propan-2-ol. Physical Chemistry Chemical Physics. 2001;3:4430-6.
[18] Izan SM, Jalil AA, Hitam CKNLCK, Nabgan W. Influence of nitrate and phosphate on silica fibrous beta zeolite framework for enhanced cyclic and noncyclic alkane isomerization. Inorganic Chemistry. 2020;59:1723-35.

[19] Aziz FFA, Jalil AA, Hassan NS, Hitam CNC, Rahman AFA, Fauzi AA. Enhanced visible-light driven multi-photoredox Cr(VI) and p-cresol by Si and Zr interplay in fibrous silica-zirconia. Journal of Hazardous Materials. 2021;401:123277.
[20] Aziz MAH, Jalil AA, Siang TJ, Hussain I, Rahman AFA, Hamdan H. Abundant Lewis acidic sites of peculiar fibrous silica zeolite X enhanced toluene conversion in side chain toluene methylation. Fuel. 2021;305:121432.
[21] Fauzi A, Jalil A, Mohamed M, Triwahyono S, Jusoh N, Rahman A, et al. Altering fiber density of cockscomb-like fibrous silica–titania catalysts for enhanced photodegradation of ibuprofen. Journal of Environmental Management. 2018;227:34-43.
[22] Siang TJ, Jalil AA, Hamid MYS. Bifunctional metal-free KAUST Catalysis Center 1 (KCC-1) as highly active catalyst for syngas production via methane partial oxidation. Materials Today Chemistry. 2022;23:100684.
[23] Firmansyah ML, Jalil AA, Triwahyono S, Hamdan H, Salleh MM, Ahmad WFW, et al. Synthesis and characterization of fibrous silica ZSM-5 for cumene hydrocracking. Catalysis Science & Technology. 2016;6:5178-82.
[24] Abdulrasheed A, Jalil A, Hamid M, Siang T, Fatah N, Izan S, et al. Dry reforming of methane to hydrogen-rich syngas over robust fibrous KCC-1 stabilized nickel catalyst with high activity and coke resistance. International Journal of Hydrogen Energy. 2020;45:18549-61.
[25] Khusnun NF, Jalil AA, Abdullah TAT, Latip SSM, Hitam CNC, Fauzi AA, et al. Influence of TiO_2 dispersion on silica support toward enhanced amine assisted CO_2 photoconversion to methanol. Journal of CO_2 Utilization. 2022;58:101901.
[26] Bahari MB, Mamat CR, Jalil AA, Shing LS, Hassan NS, Aziz FFA, et al. Enriching the methanol generation via CO_2 photoconversion over the cockscomb-like fibrous silica copper. Fuel. 2022;328:125257.
[27] Siang TJ, Jalil AA, Fatah NAA, Chung ME. Tailoring Rh content on dendritic fibrous silica alumina catalyst for enhanced CO_2 capture in catalytic CO_2 methanation. Journal of Environmental Chemical Engineering. 2021;9:104616.
[28] Hussain MK, Khalid N, Tanveer M, Kebaili I, Alrobei H. Fabrication of CuO/MoO_3 pn heterojunction for enhanced dyes degradation and hydrogen production from water splitting. International Journal of Hydrogen Energy. 2022;47:15491-504.
[29] Liu S, Yang Z, Zhao L, Zhang Y, Xing Y, Fei T, et al. Glucose-assisted combustion synthesis of oxygen vacancy enriched α-MoO_3 for ethanol sensing. Journal Alloy Compound. 2022;902:163711.
[30] Izzudin NM, Jalil AA, Ali MW, Aziz FFA, Azami MS, Hassan NS, et al. Promoting a well-dispersion of MoO_3 nanoparticles on fibrous silica catalyst via one-pot synthesis for enhanced photoredox environmental pollutants efficiency. Chemosphere. 2022;308:136456.
[31] Ibrahim M, Jalil A, Khusnun N, Fatah N, Hamid M, Gambo Y, et al. Enhanced n-hexane hydroisomerization over bicontinuous lamellar silica mordenite supported platinum (Pt/HM@ KCC-1) catalyst. International Journal of Hydrogen Energy. 2020;45:18587-99.
[32] Azami MS, Jalil AA, Hassan NS, Hussain I, Fauzi AA, Aziz MAA. Green carbonaceous material–fibrous silica-titania composite photocatalysts for enhanced degradation of toxic 2-chlorophenol. Journal of Hazardous Materials. 2021;414:125524.
[33] Myachina M, Gavrilova N, Nazarov V. Formation of Molybdenum Blue Nanoparticles in the Organic Reducing Area. Molecules. 2021;26:4438.
[34] Bahari MB, Jalil AA, Mamat CR, Hassan NS, Khusnun NF, Herrynaldi AR, et al. New insight into the mechanism of isomerization of C_5–C_7 alkanes over MoO_3/FST. Molecular Catalysis. 2023;535:112873.

[35] Sawal MH, Jalil AA, Abdullah TAT, Khusnun NF, Hassan NS, Aziz FFA, et al. Si-Ti interaction in unique morphology of fibrous silica titania photoanode for enhanced photoelectrochemical water splitting. Energy Conversion and Management. 2022;274:116456.
[36] Hitam CNC, Jalil AA, Raji YO. Fabrication of Fibrous Silica Zinc (FSZn) Composite for Enhanced Photocatalytic Desulphurization. Topics in Catalysis. 2020;63:1169-81.
[37] Azami MS, Jalil AA, Aziz FFA, Hassan NS, Mamat CR, Izzudin NM. Influence of the nitrogen pots from graphitic carbon nitride with the presence of wrinkled silica-titania for photodegradation enhancement of 2-chlorophenol. International Journal of Hydrogen Energy. 2021;48:6532-6545.
[38] Aziz FFA, Jalil AA, Triwahyono S, Mohamed M. Controllable structure of fibrous SiO_2–ZSM-5 support decorated with TiO_2 catalysts for enhanced photodegradation of paracetamol. Applied Surface Science. 2018;455:84-95.
[39] Auepattana-aumrung C, Suriye K, Jongsomjit B, Panpranot J, Praserthdam P. Inhibition effect of Na^+ form in ZSM-5 zeolite on hydrogen transfer reaction via 1-butene cracking. Catalysis Today. 2020;358:237-45.
[40] Rahman AFA, Jalil AA, Hamid MYS, Hussain I, Hassan NS, Khoja AH. Improved ethylbenzene suppression and coke-resistance on benzene methylation over metals doped fibrous silica-HZSM-5 zeolite. Molecular Catalysis. 2022;526:112370.
[41] Gao X, Chen C, Zhang W, Hong Y, Wang C, Wu G. Sulfated TiO2 supported molybdenum-based catalysts for transesterification of Jatropha seed oil: Effect of molybdenum species and acidity properties. Renewable Energy. 2022;191:357-69.
[42] Cruz MC, Sánchez-Velandia JE, Causíl S, Villa AL. Selective Synthesis of Perillyl Alcohol from β-Pinene Epoxide over Ti and Mo Supported Catalysts. Catalysis Letters. 2021;151:2279-90.
[43] Setiabudi HD, Jalil AA, Triwahyono S. Ir/Pt-HZSM5 for n-pentane isomerization: Effect of iridium loading on the properties and catalytic activity. Journal of Catalysis. 2012;294:128-35.
[44] Ma J, Qiang L-S, Wang J-F, Tang X-B, Tang D-Y. Effect of different synthesis methods on the structural and catalytic performance of SBA-15 modified by aluminum. Journal of Porous Materials. 2011;18:607-14.
[45] Lyu Y, Liu Y, Xu L, Zhao X, Liu Z, Liu X, et al. Effect of ethanol on the surface properties and n-heptane isomerization performance of Ni/SAPO-11. Applied Surface Science. 2017;401:57-64.
[46] Triwahyono S, Jalil AA, Ruslan NN, Setiabudi HD, Kamarudin NHN. C_5–C_7 linear alkane hydroisomerization over MoO_3–ZrO_2 and Pt/MoO_3–ZrO_2 catalysts. Journal of Catalysis. 2013;303:50-9.
[47] Chica A, Corma A, Miguel PJ. Isomerization of C_5–C_7 n-alkanes on unidirectional large pore zeolites: activity, selectivity and adsorption features. Catalysis Today. 2001;65:101-10.
[48] Noda LK, de Almeida RM, Probst LFD, Gonçalves NS. Characterization of sulfated TiO_2 prepared by the sol–gel method and its catalytic activity in the n-hexane isomerization reaction. Journal of Molecular Catalysis A: Chemical. 2005;225:39-46.
[49] Hattori H. Solid Acid Catalysts: Roles in Chemical Industries and New Concepts. Topics in Catalysis. 2010;53:432-8.
[50] Al-Kandari H, Mohamed AM, Al-Kharafi F, Zaki MI, Katrib A. Modification of the catalytic properties of $MoO_{2-x}(OH)_y$ dispersed on TiO_2 by Pt and Cs additives. Applied Catalysis A: General. 2012;417-418:298-305.
[51] Matsuda T, Ohno T, Hiramatsu Y, Li Z, Sakagami H, Takahashi N. Effects of the amount of MoO_3 on the catalytic properties of H_2-reduced Pt/MoO_3–SiO_2 for heptane isomerization. Applied Catalysis A: General. 2009;362:40-6.

[52] Breitkopf C, Papp H, Li X, Olindo R, Lercher JA, Lloyd R, et al. Activation and isomerization of n-butane on sulfated zirconia model systems—an integrated study across the materials and pressure gaps. Physical Chemistry Chemical Physics. 2007;9:3600-18.
[53] Ruslan NN, Fadzlillah NA, Karim AH, Jalil AA, Triwahyono S. IR study of active sites for n-heptane isomerization over MoO_3-ZrO_2. Applied Catalysis A: General. 2011;406:102-12.
[54] Liu P, Wu M-Y, Wang J, Zhang W-H, Li Y-X. Hydroisomerization of n-heptane over MoP/Hβ catalyst doped with metal additive. Fuel Processing Technology. 2015;131:311-6.
[55] Parsafard N, Peyrovi MH, Parsafard N. Pt-HMS catalyst promoted with MoO_x/ZrO_2 mixed oxides for n-heptane isomerization: catalytic performance and kinetics. Reaction Kinetics, Mechanisms and Catalysis. 2017;120:231-46.

Mechanistic studies of lower temperature isomerization of n-heptane over fibrous silica molybdenum catalyst

M.B. Bahari[c], A.A. Jalil[a,b*], C.R. Mamat[c], N.S. Hassan[a,b], M.H. Razak[a], N.M. Izzudin[a], M.A.A. Aziz[a], N.F. Khusnun[b], M.A.H.Aziz[c], A.F.A. Rahman[b], W. Nabgan[d], Saravanan Rajendran[e]

[a] *Faculty of Chemical and Energy Engineering, Universiti Teknologi Malaysia, 81310 UTM Johor Bahru, Johor, Malaysia.*

[b] *Centre of Hydrogen Energy, Institute of Future Energy, Universiti Teknologi Malaysia, 81310 UTM Johor Bahru, Johor, Malaysia.*

[c] *Faculty of Science, Universiti Teknologi Malaysia, 81310 UTM Johor Bahru, Johor, Malaysia.*

[d] *Departament d'Enginyeria Química, Universitat Rovira i Virgili, Av Països Catalans 26, 43007, Tarragona, Spain*

[e] *Departamento de Ingeniería Mec´anica, Facultad de Ingeniería, Universidad de Tarapac´a, Avda. General Vel´asquez 1775, Arica, Chile*

**To whom correspondence should be addressed,*

Aishah Abdul Jalil (Ph.D.)

Tel: 60-7-5535581 Fax: 60-7-5536165

Email: aishahaj@utm.my

Abstract

Platinum (Pt) inclusion on fibrous silica molybdenum (FSMo) and MoO_3/KCC-1 catalysts has been prepared and utilized for the lower temperature (200-350 ºC) catalytic isomerization of n-heptane. The impact of Pt inclusion towards the structure, morphology, and acid distribution of catalysts was characterized by XRD, FTIR, N_2-physisorption, Py-IR, and H_2-IR. Compared with MoO_3/KCC-1, FSMo demonstrated superior MoO_3 dispersion and amount of Lewis acid site associated with the in-situ synthesis technique. Although Pt inclusion slightly lessened acid sites due to inevitable partial coverage by the Pt cluster, the considerably higher amount of Lewis acid sites compared to Brønsted and conjugated sufficiently for generating protonic acid sites for enriching the isomerization activity. In contrast to Pt/MoO_3/KCC-1 and undoped catalysts, Pt/FSMO achieved a superior conversion of 70.9% with 63.6% isomer yield at a low temperature of 250 ºC. The 28-h stability tests demonstrated that Pt/FSMO recorded stable isomerization activity, with a superior isomer yield (~48-52%) and inferior cracking yield (<3.0%) than Pt/MoO_3/KCC-1.

Keywords: n-C_7 isomerization; MoO_3-based catalysts; Platinum; Lewis acid; Protonic acid side

1.0 Introduction

Globally, comprehensive research and development initiatives have been undertaken to produce clean gasoline with low aromatics, olefins, sulphur, and high-octane numbers, in response to growing concerns over energy and environmental issues [1]. As a result, n-alkane isomerization has gained popularity as a safe and environmentally friendly method for enhancing gasoline quality [2]. This pathway allows n-alkanes with a linear carbon chain to be converted into branched isomers with a high research octane number (RON) [3, 4]. So far, tremendous effort has been put forth in researching light alkane isomerization since this compound processing has been industrialised. Yet, this technique has not been utilized for *n*-heptane and heavier alkanes due to the higher tendency of excessive development of cracking products as the conversion rate increases, leading to the deactivation of the catalyst due to the accumulation of coke on the surface's catalysts [5]. Hence, considering potential implementation, it is critical to look for relatively efficient and selective catalysts for heavy n-heptane isomerization while concurrently limiting cracking activities.

Bifunctional heterogeneous catalyst materials consisting of acidic supporting materials as well as hydrogenation/hydrogenation metal sites are among the popular catalysts used for the catalytic acid reaction [6, 7]. Both metallic and acidic functions influence the catalyst's properties and facilitate the alkane hydro-conversion. For instance, metal sites could generate carbonium ions via alkane dehydrogenation, a crucial intermediate species for initiating isomerization and cracking [8]. Once the acidity of the catalyst is mild, and the dehydrogenation activity of metal is substantial, a high yield of isomers is generated. In addition, when the dehydrogenation activity is more significant, unsaturated products are more hydrogenated, thus, inhibiting the escape acid-catalyzed skeleton rearrangement and cracking [9]. Throughout the scientific literature, *n*-alkane isomerization has made considerable use of

catalysts such as noble metals supported on microporous and mesoporous materials. In fact, it was found that the hydrogen atom spillover mechanism used by bifunctional heterogeneous catalysts could strongly induce isomerization [10]. Numerous acid-catalyzed reactions using various types of catalysts, like Pt/MoO_3 [11-13], Pt/WO_3-ZrO_2 [14], MoO_3/MSN [15], and Zn/HZSM-5 [10], have been explored for their spillover mechanisms.

Recently, the potential of the MoO_3 type catalysts has been extensively explored for a wide range of catalytic processes like methanation, olefin metathesis, alcohols oxidation, and isomerization accredited to MoO_3's exceptional features, including excellent stability and regeneration performance [16]. In addition, MoO_3 possessed both Lewis and Bronsted acid sites, which is crucial for *n*-alkane isomerization and provides superior selectivity for heptane isomerization compared to conventional catalysts. Incorporating second material as active sites into bifunctional catalysts has aroused considerable attention in recent years owing to the positive effects on isomerization performance, isomer selectivity, as well as stability. Second Noble materials like Pd and Pt have been extensively studied, attributed to their hydrogen spillover capability, boosting the isomerization activity. Indeed, the combination between Pt and MoO_3 in a hydrogen atmosphere can generate several active species, including H_xMoO_3 and MoO_2, that are utilized for isomerization [11, 17]. Previous work has demonstrated that incorporating Pt and MoO_3 into diverse supporting materials effectively improved n-heptane isomerization performance [11, 13]. Regrettably, it should be noted that there is a paucity of literature focusing on the usage of catalysts at low operating temperature.

Creating support with a dendrimer fibrous structure has recently received much attention [18]. This strategy can produce an ideal support material possessing vast surface area, tuneable pore volume, conveniently reachable inner surface, as well as superior thermal stability [19-21]. In fact, this approach has resulted in a positive effect on the catalytic activity of all catalytic pathways, including isomerization [4], methanation [22], cumene cracking [23],

and dry reforming [24]. According to the researchers, the improvement was attributable to the enhanced accessibility of active areas within this particular shape. Inspired by the previous study, we synthesized fibrous silica-molybdenum trioxide (FSMo) supported platinum (Pt) and assessed their capability in *n*-heptane isomerization at low reaction temperature for the first time. The fibrous silica in the Pt/FSMo catalyst induces Si-O-Mo formation to enhance Lewis acid site quantity, which will cause a growth in protonic acid site generation, thus enriching *n*-heptane isomerization activity. The physicochemical features of the studied catalysts were analysed in detail via XRD, N_2 physisorption and several in-situ IR analysis. The isomerization pathway over Pt/FSMo catalyst is also elucidated.

2.0 Experimental

2.1 MoO_3-based catalysts synthesis

Fibrous silica-molybdenum (FSMo) and KCC-1 were prepared corresponding to the microemulsion approach as detailed in the literature [25, 26]. In brief, a homogeneous solution consisting of CTAB and urea was acquired by mixing and stirring both chemicals in distilled water for 15 min (25ºC). Thereafter, butanol, TEOS, and toluene were poured into the resulting mixture under continuous agitation for one hour at ambient temperature. The mixture was further agitated at ambient temperature for two hours to guarantee TEOS was hydrolyzed entirely prior to the six-hour hydrothermal treatment in microwave irradiation (120 ºC, 400 W). Afterwards, the acquired solution was air-dried in an oven (24 h, 110 ºC) to eradicate the moisture before furnace-calcination (6 h, 550 ºC) to gain desired FSMo. On the contrary, for KCC-1 support production, TEOS was dropped along with butanol and toluene before being

treated with a similar condition for hydrothermal treatment, air-drying, and furnace-calcination.

The incipient wetness impregnation technique, as reported by Siang et al. [27], was applied in this work to generate Pt/FSMo and MoO_3/KCC-1 catalysts. For KCC-1 supported MoO_3 catalyst, a calculated amount of ammonium heptamolybdate ($[NH_4]_6Mo_7O_{24}$) as the metal precursor and KCC-1 support were separately dissolved in the deionized water prior to the impregnation step. After both solutions were mixed and agitated at ambient temperature for four hours, the resulting mixture was further air-dried in an oven (24 h, 110 ºC) and subsequently underwent furnace-calcination (6 h, 550 ºC), which yielded MoO_3/KCC-1. A similar approach as those stated earlier was employed to prepare Pt/FSMo using chloroplatinic acid hexahydrate ($H_2PtCl_6 \cdot 6H_2O$) as the metal precursor over FSMo support. For Pt/MoO_3/KCC-1 catalyst preparation, the sequential incipient wetness impregnation technique was employed by discretely dissolved $H_2PtCl_6 \cdot 6H_2O$ and as-synthesized MoO_3/KCC-1 in deionized water. Afterwards, both dissolved materials were combined, agitated, dried, and calcined, similar to those earlier impregnation steps to acquire Pt/MoO_3/KCC-1.

2.3 Characterizations of MoO_3-based catalysts

The crystalline structure of studied catalysts was assessed by X-ray diffractogram (2θ = 20-85°, step size = 0.02) on a Bruker Advance D8 diffractometer equipped with Cu Ka radiation (λ =0.154 nm, V = 40 kV, I = 40m A). The Barrett-Joyner-Halenda (BJH) and Brunauer-Emmet-Teller (BET) techniques were applied to measure the catalyst's surface area and pore properties using liquid nitrogen at -196 °C in a Beckman Coulter SA3100 unit. The one-hour-outgassed treatment was initially employed at 300 °C prior to the nitrogen adsorption at 77 K for eradicating the moisture and contaminants. The functional groups of the studied

catalysts were appraised via the FTIR-KBr approach at the range of 1600-400 cm^{-1} with 5 cm^{-1} resolutions on the FT-IR spectrometer unit (Agilent Cary 660). The acidity of studied catalysts was scrutinized through Py-IR adsorption on stainless-steel cells with two CaF2 windows sealed. Initially, the tested catalysts were pelletized before exposing them to 4 Torr of pyridine stream for a quarter-hour at 150 °C. Afterwards, the desorption of pyridine from tested catalysts was carried out at a different temperature within 150-350°C. H_2-IR adsorption was also operated in similar equipment for Py-IR adsorption. After activation treatment, the tested catalysts were cooled down to room temperature before being subjected to 20 Torr of the hydrogen stream under rising temperature up to 350 °C.

2.4 n-C_7 Isomerization evaluation

The micro-catalytic pulse reactor was utilized to evaluate *n*-heptane isomerization within 200-350 °C. About 0.2 g of the studied catalyst was employed in the reactor, followed by exposure to the 100 ml min^{-1} of O_2 stream (1 h, 400 °C) and then 100 ml min^{-1} H_2 stream (3 h, 400 °C) as the pre-treatment step. Subsequently, the tested catalyst was cold down in a similar H_2 stream to reach 150 °C. After stabilizing and reaching the necessary conditions, about two µmol of n-C_5 was driven into the reactor filled with an H_2 stream (100 ml min^{-1}) to commence the isomerization process. An online gas chromatograph (Agilent 6090N, FID, HP-5), connected with a utilized micro-catalytic pulse reactor, scrutinized the isomerization product. The isomerization product was confined using N_2 (77 K) before being flash-evaporated into the gas chromatograph system. The isomerization activity was estimated based on the conversion (*X*), yield (*Y*), and selectivity (*S*), as expressed in Eqs. (1)-(3).

$$X_i(\%) = \frac{\sum C_i - C_{r,i}}{C_i} \times 100\% \quad (1)$$

$$S_i(\%) = \frac{C_i}{\sum C_i - C_{r,i}} \times 100\% \quad (2)$$

$$Y_i = \frac{X_i \times S_i}{100} \quad (3)$$

Where C_i = concentration for a specific product and $C_{r,i}$ = concentration of residual of n-heptane species, in weight percent unit.

3.0 Results and Discussion

3.1 Characterization analysis

XRD diffractograms for commercial MoO_3 and generated catalysts are shown in Figs. 1A-B. All of the prepared catalysts showed a clear peak at 2θ = 10°-70° on the plot. The XRD pattern of the MoO_3 catalyst demonstrated that it possesses an orthorhombic structure consistent with standard data (JCPDS Card No: 050508) [28]. The crystallite peaks corresponded to the MoO_3 witnessed at an angle of 2θ about 12.9° (020), 23.4° (110), 25.8° (040), 27.4° (021), 33.7° (111), 39.0° (041), 46.1° (200), and 49.4° (002) in FSMo and MoO_3/KCC-1 [29]. The inferior intensity of crystallite peaks of FSMO than MoO_3/KCC-1 catalyst, indicating that the in-situ synthesis strategy for generating FSMo promoted the well-distribution of Mo on the Si framework in comparison to MoO_3/KCC-1 prepared via the incipient wetness impregnation approach [30]. Furthermore, due to the small size of the Pt species dispersed on the FSMo and MoO_3/KCC-1, possibly below than XRD detection limit, further explained for no visible diffraction peaks assignable to Pt species over Pt/FSMo and Pt/ MoO_3/KCC-1 [31].

The FTIR spectra (1400-400 cm^{-1}) of the functional groups owned by studied catalysts are depicted in Fig. 2. Evidently, all the studied catalysts displayed five identical IR bands ranging from 1095 cm^{-1} to 467 cm^{-1}. The absorption peaks appeared at a wavenumber of 1095 cm^{-1}, 956 cm^{-1}, 802 cm^{-1}, and 467 cm^{-1} are linked to the vibration of asymmetric Si-O-Si, external Si-OH, symmetric Si-O-Si, and bending Si-O-Si, respectively [32]. Meanwhile, absorption peaks identified at a wavenumber of 902 cm^{-1} overall studied catalysts signified weak Mo=O vibration [33, 34]. Following the modification of MoO_3 into FSMO, a drop in the intensity for the IR band at 956 cm^{-1} (external Si-OH vibration) for FSMO compared to MoO_3/KCC-1 suggesting that more replacement of -H by Mo ions to form Si-O-Mo, associated with the alternately aligned SiO_2 and MoO_3 in the fibrous structure. As a consequence, this improvement could strengthen the interaction of MoO_3-SiO_2. This observation was also reported by Sawal et al. [35] and Hitam et al. [36]. Remarkably, the FTIR spectrum of $FSMO_3$ was almost identical to that of Pt/$FSMO_3$, revealing no significant changes towards the silicate framework of $FSMO_3$ after Pt incorporation. Apart from that, it is apparent from these FTIR spectra that most of the IR bands for FSMO and MoO_3/KCC-1 catalysts experienced a slight decrease in intensity compared to Pt-loaded catalysts, indicating the successful impregnation of Pt over the tested catalysts, creating new interaction between Pt and SiO_2.

Further investigation was performed using N_2 physisorption analysis to examine synthesized catalysts' textural properties; the results are presented in Fig. 3. As can be observed, all the prepared catalysts demonstrated a type IV isotherm profile with a typical H3 hysteresis loop, confirming the mesoporous structure characteristic of the synthesized catalysts (Fig. 3A) [30]. In addition, in the absence of Pt element, both FSMo and MoO_3/KCC-1 catalysts exhibited comparable N_2 uptakes. However, when Pt was loaded onto the catalyst surface, the relative pressure of N_2 uptakes for Pt/MoO_3/KCC-1 increased substantially, while Pt/FSMo catalyst demonstrated an insignificant change. This result may be explained by the fact that

high interaction between the Pt element and MoO_3 of Pt/MoO_3/KCC-1 reduced the pore blockage of the MoO_3 on the mesopore of the KCC-1 [36]. Besides, the total pore volume for MoO_3/KCC-1 catalyst was increased after adding Pt (Table 1) which indirectly supported the statement mentioned earlier. Meanwhile, for Pt/FSMo catalyst, the pore volume was slightly decreased compared to the FSMo catalyst, suggesting the filling of Pt inside the FSMo mesopore [30].

Barrett-Joyner- Halenda (BJH) approach was applied to assess the average pore diameter, as shown in Fig. 3B. The BJH pore size distribution demonstrated the pore diameter of the synthesized catalysts placed within 3-40 (Å), showing the intrinsic of mesopores features. It is worth noting that the pore distribution of FSMo and KCC-1 supported MoO_3 catalysts was considerably grown by adding Pt, probably due to the high mesoporous of Pt that created inter-dendrimer distances [37]. For a better understanding of the textural properties of as-prepared catalysts, the results were tabulated and presented in Table 1. As noticed, the surface area for both FSMo (114.6 m^2/g) and MoO_3/KCC-1 (221.3 m^2/g) was reduced considerably after adding Pt, suggesting that pores of FMSO and MoO_3/KCC-1 catalysts was partially blocked by Pt particles [38]. This trend further inferred that the alteration of catalyst structure could lead to surface area changes.

The efficacy of the isomerization reaction was considerably linked to the number and intensity of the surface acidity in catalysts. Thus, Py-IR measurement was applied to assess the distribution of Lewis and Brønsted acidic sites over activated catalysts at different temperatures (150-250 ºC), and the Py-IR spectra are illustrated in Fig. 4. As can be seen, all of the studied catalysts disclosed three IR bands ranging within 1570-1420 cm^{-1}. It was noted that IR bands spotted at 1454 cm^{-1} and 1539 cm^{-1} belonged to pyridinium ions adsorption on Lewis and Brønsted acid sites, respectively [39, 40]. In addition, the appearance of IR band at a wavenumber of 1488 cm^{-1} over all tested catalysts related to Brønsted and Lewis acid sites

combination [41, 42]. Interestingly, by comparing FSMO and MoO_3/KCC-1, it was noticed that Lewis acid sites intensity for FSMO was considerably higher than KCC-1 supported MoO_3 catalysts, possibly ascribed to the more replacement of -H (from Brønsted) by Mo ions in forming Si-O-Mo (Lewis acid sites), resulted from the fibrous framework, in line with FTIR finding. The decline in Lewis and Brønsted acid site intensity was witnessed after Pt was impregnated onto FSMO and MoO_3/KCC-1, suggesting the inevitable partial coverage of acidic sites by the Pt cluster. A comparable phenomenon was claimed by Setiabudi et al. [43] and Teh et al. [5] during the isomerization over Ir/Pt-HZSM5 and Pt/MoO_3-HBEA catalysts, respectively.

The impact of outgassed temperature (150-350 ºC) towards the distribution of acidic sites on studied catalysts is also elucidated in Fig. 4. The pyridine molecules adsorbed on weak acid sites typically desorbed at a lower temperature whilst higher outgassing temperature is required for desorbing pyridine molecules for strong acid sites. All tested catalysts appeared to demonstrate intense interaction between pyridine and acidic sites at 150 ºC and remained firm at the outgassing temperature of 150 ºC. The considerable decline in the intensity of acidic sites for all studied catalysts was evidenced along with the rising outgassing temperature of up to 350 ºC, signifying that weak-to-moderate Brønsted and Lewis acid sites are dominantly located on those catalysts. This outcome also accords with the trends observed by other studies by Fatah et al. [15] and Ma et al. [44] during the Py-IR evaluation over Pt/MSN, MoO_3/MSN, and Al/SBA catalysts, respectively. Previous studies on isomerization have noted that the more significant amount and intensity of acid sites of catalysts favour cracking instead of isomerization reaction [5, 45]. Thus, the optimum amount with moderate acid sites is preferable for enhanced isomerization.

Fig.5 disclosed the Py-IR spectra in the 1600-1400 cm^{-1} when the pyridine pre-adsorbed catalysts were heated in H_2 gas at elevated temperatures. The heating of all catalysts under H_2

gas exposure modified the intensity of Lewis and Bronsted acid sites at 1446 cm^{-1} and 1538 cm^{-1}, respectively. Particularly, the intensity of Lewis acid sites declined with the simultaneous rise in the Bronsted acid sites, indicating the formation of protonic acid sites from hydrogen atoms spillover [4]. In general, protonic acid sites formed through interconversion of the Lewis acid sites. In this study, the protonic acid site formation rate is higher in all catalysts at lower temperatures (250-300 °C), as presented in Fig. 6. For FSMo and MoO_3/KCC-1, the formation of protonic acid sites was probably due to the interaction of the Mo atom with the proton in the form (MoO_x)-$(H_y)^+$) that generated from releasing of the electron by atomic hydrogen, as similarly reported by previous studies [15]. Interestingly, adding Pt into both catalysts significantly increased the protonic acid site formation rate, especially at low operating temperatures. These results indicated that Pt heightened the interaction of the hydrogen atom with the surface of FSMo and MoO_3/KCC-1. This phenomenon has also been observed in Pt/WO_3-ZrO_2 catalysts by Triwahyono et al. [46].

3.2 n-C_7 Isomerization performance

Fig. 7 depicts the isomerization activity of FSMO, MoO_3/KCC-1, Pt/FSMO, and Pt/MoO_3/KCC-1 in *n*-heptane isomerization within 200-350 ºC. Notably, all catalysts suffered a decrement in the yield of isomers along with the rise in operating temperature, which attained optimum yield at 200-250 ºC and decreased above 250 ºC. This trend was associated with the domination of cracking reaction compared to heptane isomerization at a higher temperature. It is interesting to note that FSMO presented a superior *n*-heptane conversion (53-55%) and yield of isomers (46-52%) compared to MoO_3/KCC-1, regardless of reaction temperature owing to considerably greater average pore size of FSMO (19.8 nm > 12.4 nm), as provided in Table 1. The enlargement in pore size was believed to minimize the transport restriction throughout the

catalysts as well as improve the diffusion steps [47, 48]. Additionally, the high isomerization activity of FSMO than MoO_3/KCC-1 was probably related to possessing a moderate amount of weak Bronsted acid sites. This finding is accorded with the result from Py-IR with different outgassing temperatures (Fig. 4), which showed that FSMO possessed a lower amount of Bronsted acid sites than KCC-1 supported MoO_3 catalysts since there was more replacement of -H (from Brønsted) by Mo ions in forming Si-O-Mo (Lewis acid sites). Consequently, this domination facilitated the formation of the protonic acid site via H_2 dissociation and spillover, resulting in high isomerization activity. This trend was also evident from the experimental work of Triwahyono et al. [4], in which the modification of Y zeolite (HY) into fibrous silica@Y zeolite for C_5-C_7 isomerization.

Improvement in conversion and yield of isomer was noticed, especially at a lower temperature (<350 ºC) after incorporating Pt over FSMO and MoO_3/KCC-1 (Fig. 7). The results demonstrated that Pt/FSMO achieved optimal conversion of 70.9% with 63.6% isomer yield at a temperature of 250 ºC. Instead, Pt/MoO_3/KCC-1 recorded a maximum conversion of 61.7% with the yield of an isomer of 56.5% at 200 ºC. The enhancement in the isomerization activity after Pt addition, especially at low temperatures, was plausibly attributed to the considerably higher amount of Lewis acid sites than Brønsted and conjugated acid sites as demonstrated in Py-IR (cf. Fig. 4), appropriately sufficient in generating protonic acid sites for enriching the isomerization activity. Furthermore, this improvement could be linked to new active site species generated from the interaction of Pt-support lattice defects [5]. Thus, the addition of Pt over FSMO and MoO_3/KCC-1 could facilitate the activation of hydrogen molecules via dissociation, enhancing the spillover process and thus enriching the formation of protonic acid sides and hydrides for generating more isomer products. Interestingly, the yield of cracking exhibited by Pt/FSMO is slightly lower compared to FSMO at 350 ºC, suggesting that Pt doped over FSMO effectively suppressed the binding interaction between FSMO and

atomic hydrogen, thus enriching the formation of hydride ions that are responsible for the generation of the desired isomerization products [17]. In contrast, the high yield of cracking witnessed at 350 ºC for Pt/MoO_3/KCC-1 probably indicates that Pt incorporation could not restrain the binding interaction between support and spillover hydrogen atom, thus lowering the hydride generation. At low hydride availability, the hydrogen atoms' migration will occur slowly compared to the β-fission, favouring more cracking products than isomers [49].

Increased isomerization activity with the incorporation of Pt is also consistent with those of Al-Kandari et al. [50], who have evaluated the catalyst's isomerization activity over TiO_2-supported MoO_3. They found that Pt incorporation effectively improved the bifunctional metallic-acidic system of the MoO_3/TiO_2 catalyst, causing an improvement in *n*-heptane isomerization activity at 573 K. In different work, Matsuda and coworkers [51] highlighted that the enhancement of n-heptane isomerization could attain by introducing Pt over the reduce MoO_3 catalysts. The authors noticed that this effort could produce acidic molybdenum oxyhydride (MoO_xH_y), a crucial active site for enhancing the isomerization performance. Teh et al. [5] also discovered a significant improvement in n-heptane isomerization after incorporating Pt on the MoO_3-HBEA catalyst, accredited to the role of Pt in dissociating hydrogen molecule, suppressing the MoO_3-spillover hydrogen atom interaction, while enriched protonic acid sites quantity.

The stability performance of Pt/FSMO and Pt/MoO_3/KCC-1 in *n*-heptane isomerization under 28 h time-on-stream with intervals of 15 min for each dose was plotted in Fig. 8. Although Pt/MoO_3/KCC-1 recorded superior conversion (>~60.0%) as compared to Pt/FSMO, this catalyst experienced unsteady isomerization activity within 28 h reaction. This phenomenon probably resulted from the high cracking side reaction, which could deactivate the catalysts as a consequence of high coke accumulation. On the contrary, Pt/FSMO recorded stable isomerization activity, especially with a better isomer yield (~48-52%) and a lower

cracking yield (<3.0%). This trend proves the efficient role of Pt in enhancing the Lewis acid site of the catalyst for generating essential protonic acid, minimizing the strong support-spillover hydrogen atom interaction, and assisting in lessening the coke accumulation via hydrogenation. Thus, it is noteworthy that Pt/FSMO catalysts have excellent potential for long-term isomerization reactions.

3.4 Proposed reaction pathway

Based on the characterizations and *n*-heptane isomerization test, as mentioned before, it can be evidenced that MoO_3 modification into the fibrous structure of support with silica ($FSMO_3$), along with the incorporation of Pt element, could enrich the generation of Lewis acid sites, thus, aiding in essential protonic acid sites generation at low temperature. This factor further explains the excellent performance of Pt/FSMO catalyst on *n*-heptane isomerization at a lower temperature. In order to comprehend the isomerization mechanism, the proposed reaction pathway for *n*-heptane isomerization over Pt/FSMO is clarified in Fig. 9.

At the initial pathway, the pre-treatment of Pt/FSMO in the H_2 stream resulted in the instigation of Pt-oxide into metallic Pt, the crucial hydrogen activation sites. The H_2 molecules adsorbed on metallic Pt were further dissociated into two species of hydrogen atoms. This dissociation step is crucial in isomerization since it contributes to acid site generation, favouring the isomer generation instead of the cracking and polymerization of *n*-C_7 via ß-scission [4, 52]. After splitting, the produced hydrogen atom was spilt over onto the acidic surface of FSMO and further diffused towards the Lewis acid sites. The spilt over of hydrogen atoms then transferred an electron towards Lewis acid sites and bonded with Brønsted sites of FSMO for forming protonic acid site (B-H^+ species). The generated protonic acid sites then transferred protons to *n*-heptane, resulting in the formation of heptyl carbenium ion (*n*-C_7^+)

species. Afterwards, the accepted proton in the carbenium ion was moved along the hydrocarbon chain, forming the iso-heptyl carbenium ion (*i*-C_7^+) species. Simultaneously, the electron confined by the Lewis acid sites was further reacted with another split hydrogen atom to become a hydride ion and attached to the Lewis acid site (L-H^-). Then, the produced L-H^- species further interacted with *i*-C_7^+ species contributing to the generation of the desired isomerization products. This proposed mechanism further proved that isomerization yield was strongly influenced by the protonic acid sites and hydrate ions created from H_2 dissociation in the presence of Pt. However, according to Hattori et al. [49], if there were excessive hydride species during the reaction, the concentration of carbenium ions would considerably drop, lowering the isomerization activity.

3.5 Comparative analysis

In order to evaluate the competency of our generated MoO_3-based catalysts, a comparative analysis (cf. Table 2) towards the reported MoO_3-based catalyst's activity over *n*-heptane isomerization was conducted. Fatah et al. [15] compared the isomerization activity of over MoO_3- and Pt- supported with MSN in the system consisting of H_2 or N_2 as the carrier. The high performance of MoO_3-supported with MSN conducted in the H_2 system was recorded with mono- and di-branched iso-heptane, which yielded about 81.3 and 12.4%, respectively, resulting from $(MoO_x)^-(H_y)^+$ active sites formation. On the other hand, the authors claimed that the incompetence of the Pt- supported with MSN to generate protonic acid sites led to poor isomerization activity. The author also evaluated the isomerization performance over MoO_3 supported by KCC-1, incorporating the phosphorous element [16]. The generation of $(MoO_x)^-(H_y)^+$ active site along with the involvement of acidic centres from phosphorus inclusion and MoO_3, caused the improvement in the rate of n-heptane conversion.

In another effort, Ruslan et al. [53] investigated the role of the acid site of MoO_3-ZrO_2 catalysts toward n-heptane isomerization activity. Notably, the existence of the ZrO_2 tetragonal phase in the catalysts contributed to enhancement in the number of Lewis acid sites, easing active protonic acid sites generation, thus responsible for the improvement of isomerization activity and stability. Nevertheless, the authors witness superior cracking activity compared to isomerization, which gradually increases with rising temperature from 300-400 ^oC. Besides, Matsuda et al. [51] emphasized the acid site's role and their impact on isomerization performance over Pt/MoO_3-SiO_2. They concluded that the isomerization selectivity of Pt/MoO_3-SiO_2 was enhanced from 88.7-97.8% by raising the amount of MoO_3 employed from 20-100wt%, related to the growth in the number of acid sites. Meanwhile, the cracking selectivity of Pt/MoO_3-SiO_2 was significantly reduced from 10.7% to 1.9% with the rising MoO_3 loading.

Liu et al. [54] stated that HBEA zeolite-supported molybdenum phosphide (MoP) demonstrated superior isomerization selectivity (67.8%) compared to tungsten phosphide supported on Hβ (50.1%) and HMCM22 (64.2%). The authors also proposed that doping Ce, Ni, and Cr elements over MoP/Hβ substantially enriched the activity with Cr-promoted catalyst promoted the superior isomerization selectivity around 73.1%, owing to the increment in the density of strong acid sites of MoP/Hβ. Works by Sakagami et al. [11] and Parsafard et al. [55] revealed a positive impact towards isomerization activity over MoO_3 and ZrO_2-HMS catalysts, respectively, accredited to the presence of Pt, which enhances protonic acid site generation via H_2 dissociation and spillover phenomenon. This trend is in accordance with our findings. However, the negative impact of Pt incorporation was experienced by Triwahyono et al. [46] over MoO_3-ZrO_2. The authors justified that although Pt addition improved the hydrogen adsorption rate, Pt addition has caused the intensification of Lewis acid sites instead of forming more active protonic aicd sides, consequently lowering the isomerization activity.

Table 2 shows that our generated catalysts exhibited better or comparably to other MoO_3-based catalysts that have been utilized for the isomerization of n-heptane, especially in conversion and isomerization selectivity. Indeed, the inferior cracking selectivity of studied catalysts compared to the literature indicates that all generated catalysts are favoured to isomerization activity compared to cracking. The outstanding performance of these generated catalysts, despite the absence of Pt, is ascribed to the fibrous silica morphology, which contributes to the formation of more Si-O-Mo for enriching Lewis acid sites quantity, causing growth in protonic acid sites generation, hence, enhancing the isomerization activity. Moreover, after Pt was doped, the enhancement of the Lewis acid site of the catalyst for generating essential protonic acid was evidenced, assisting in suppressing the strong support-spillover hydrogen atom interaction and lowering the coke accumulation. Thus, isomerisation activity improved, especially at the lower reaction temperature.

4.0 Conclusion

The impact of Pt inclusion towards physiochemical characteristics and isomerization activity of synthesized MoO_3-based catalysts (FSMO and MoO_3/KCC-1) were appraised and compared within this study. XRD results indicated that the in-situ synthesis strategy effectively improved the distribution of Mo particles in the Si framework than via incipient wetness impregnation. Additionally, the in-situ synthesis strategy promotes Si-O-Mo formation, associated with the alternately aligned SiO_2 and MoO_3 in the fibrous structure, strengthening MoO_3-SiO_2 interaction, as proved in FTIR analysis. Consequently, Py-IR analysis revealed that Lewis acid sites intensity for FSMO was considerably higher than KCC-1 supported MoO_3 catalyst, ascribed to the more replacement of -H (from Brønsted) by Mo ions in forming Si-O-

Mo (Lewis acid sites). Nevertheless, it is noteworthy that Pt inclusion over FSMO and MoO_3/KCC-1 lessened those acid sites owing to the inevitable partial coverage by the Pt cluster.

The isomerization tests revealed enlargement in pore size, and the possession of a moderate amount of weak Bronsted acid sites contributed to the superior n-heptane conversion (53-55%) and yield of isomers (46-52%) for FSMO compared to MoO3/KCC-1, regardless of reaction temperature. Meanwhile, incorporating Pt over FSMO and MoO3/KCC-1 improved the conversion and yield of isomer, especially at a lower temperature (<350 ºC), by achieving optimal conversion of 70.9% with 63.6% isomer yield at a temperature of 250 ºC. At the same time, Pt/MoO_3/KCC-1 recorded a maximum conversion of 61.7% with the yield of an isomer of 56.5% at 200 ºC. This trend was plausibly accredited to the considerably greater amount of Lewis than Brønsted and conjugated acid sites, which is sufficient to generate protonic acid sites for enriching the isomerization activity. Pt/FSMO recorded stable isomerization activity within 28 h, with a better isomer yield and a lower cracking yield than Pt/MoO_3/KCC-1 due to the efficient role of Pt in lessening the coke accumulation via hydrogenation. The findings of this study demonstrated the potential of Pt/FSMO as the catalyst for isomerization reactions.

Conflict of Interest

The authors hereby declare no conflict of interest for the research work reported in this manuscript.

Authorship contribution

M.B. Bahari: Project administration, Visualization, Writing - Original Draft, Methodology, **A.A. Jalil:** Project administration, Funding acquisition, Conceptualization, Visualization, Supervision, **N.S. Hassan:** Visualization, Writing - Original Draft, **MH Razak:** Investigation**,** Formal analysis, **N.M. Izzudin:** Investigation**,** Formal analysis, **NF. Khusnun:** Visualization, Writing - Original Draft**, M.A.H. Aziz**: Investigation**,** Formal analysis, **A.F.A. Rahman:** Investigation**,** Formal analysis, **W. Nabgan:** Investigation**,** Formal analysis, **Saravanan Rajendran:** Investigation**,** Formal analysis,

Acknowledgement

We are grateful for the financial support from Universiti Teknologi Malaysia (UTM) for the UTM Fundamental Research (No.22H51) and Professional Development Research University grant (No. 05E72).

References

[1] Smolikov MD, Shkurenok VA, Bikmetova LI, Prosvirin IP, Gulyaeva TI, Bukhtiyarov AV, et al. Effect of hydrogen reduction and palladium promotion of tungstate-modified zirconia on isomerization of heptane. Molecular Catalysis. 2022;529:112527.

[2] Ali NS, Alismaeel ZT, Majdi HS, Salih HG, Abdulrahman MA, Saady NMC, et al. Modification of SBA-15 mesoporous silica as an active heterogeneous catalyst for the hydroisomerization and hydrocracking of n-heptane. Heliyon. 2022;8:e09737.

[3] Saginayev A, Dosmurzina E, Apendina A, Dossanova B, Imangaliyeva B. Development of individual approaches to the use of the gasoline fraction as a raw material for the process of hydrocatalytic isomerization. Materials Science for Energy Technologies. 2022.

[4] Triwahyono S, Jalil AA, Izan SM, Jamari NS, Fatah NAA. Isomerization of linear C5–C7 over Pt loaded on protonated fibrous silica@Y zeolite (Pt/HSi@Y). Journal of Energy Chemistry. 2019;37:163-71.

[5] Teh LP, Setiabudi HD, Sidik SM, Annuar NHR, Jalil AA. Synergic role of platinum (Pt) and molybdenum trioxide (MoO3) promoted HBEA zeolite towards n-heptane isomerization. Materials Chemistry and Physics. 2021;263:124406.

[6] Ono Y. A survey of the mechanism in catalytic isomerization of alkanes. Catalysis today. 2003;81:3-16.

[7] Samad JE, Blanchard J, Sayag C, Louis C, Regalbuto JR. The controlled synthesis of metal-acid bifunctional catalysts: The effect of metal: acid ratio and metal-acid proximity in Pt silica-alumina catalysts for n-heptane isomerization. Journal of catalysis. 2016;342:203-12.
[8] Blomsma E, Martens J, Jacobs P. Isomerization and hydrocracking of heptane over bimetallic bifunctional PtPd/H-beta and PtPd/USY zeolite catalysts. Journal of Catalysis. 1997;165:241-8.
[9] Sabyrov K, Musselwhite N, Melaet G, Somorjai GA. Hydroisomerization of n-hexadecane: remarkable selectivity of mesoporous silica post-synthetically modified with aluminum. Catalysis Science & Technology. 2017;7:1756-65.
[10] Triwahyono S, Jalil AA, Mukti RR, Musthofa M, Razali NAM, Aziz MAA. Hydrogen spillover behavior of Zn/HZSM-5 showing catalytically active protonic acid sites in the isomerization of n-pentane. Applied Catalysis A: General. 2011;407:91-9.
[11] Sakagami H, Ohno T, Takahashi N, Matsuda T. The effects of Na loading on catalytic properties of H2-reduced Pt/MoO3 for heptane isomerization. Journal of Catalysis. 2006;241:296-303.
[12] Triwahyono S, Jalil AA, Timmiati SN, Ruslan NN, Hattori H. Kinetics study of hydrogen adsorption over Pt/MoO3. Applied Catalysis A: General. 2010;372:103-7.
[13] Matsuda T, Sakagami H, Takahashi N. H2-reduced Pt/MoO3 as a selective catalyst for heptane isomerization. Catalysis today. 2003;81:31-42.
[14] Cheng TX, Kabashima H, Hattori H. Effects of hydrogen and hydrogen sulfide on cumene cracking catalyzed by Pt/WO3-ZrO2. Control of acidic and metallic functions. Reaction Kinetics and Catalysis Letters. 2000;69:201-7.
[15] Fatah NAA, Triwahyono S, Jalil AA, Ahmad A, Abdullah TAT. n-Heptane isomerization over mesostructured silica nanoparticles (MSN): Dissociative-adsorption of molecular hydrogen on Pt and Mo sites. Applied Catalysis A: General. 2016;516:135-43.
[16] Fatah NAA, Triwahyono S, Jalil AA, Salamun N, Mamat CR, Majid ZA. n-Heptane isomerization over molybdenum supported on bicontinuous concentric lamellar silica KCC-1: Influence of phosphorus and optimization using response surface methodology (RSM). Chemical Engineering Journal. 2017;314:650-9.
[17] Matsuda T, Uchijima F, Sakagami H, Takahashi N. H 2-reduction of Pt/MoO 3 to MoO x with a large surface area and its catalytic activities for the conversions of heptane and propan-2-ol. Physical Chemistry Chemical Physics. 2001;3:4430-6.
[18] Izan SM, Jalil AA, Hitam CKNLCK, Nabgan W. Influence of nitrate and phosphate on silica fibrous beta zeolite framework for enhanced cyclic and noncyclic alkane isomerization. Inorganic chemistry. 2020;59:1723-35.
[19] Aziz FFA, Jalil AA, Hassan NS, Hitam CNC, Rahman AFA, Fauzi AA. Enhanced visible-light driven multi-photoredox Cr(VI) and p-cresol by Si and Zr interplay in fibrous silica-zirconia. Journal of Hazardous Materials. 2021;401:123277.
[20] Aziz MAH, Jalil AA, Siang TJ, Hussain I, Rahman AFA, Hamdan H. Abundant Lewis acidic sites of peculiar fibrous silica zeolite X enhanced toluene conversion in side chain toluene methylation. Fuel. 2021;305:121432.
[21] Fauzi A, Jalil A, Mohamed M, Triwahyono S, Jusoh N, Rahman A, et al. Altering fiber density of cockscomb-like fibrous silica–titania catalysts for enhanced photodegradation of ibuprofen. Journal of environmental management. 2018;227:34-43.
[22] Siang TJ, Jalil AA, Hamid MYS. Bifunctional metal-free KAUST Catalysis Center 1 (KCC-1) as highly active catalyst for syngas production via methane partial oxidation. Materials Today Chemistry. 2022;23:100684.
[23] Firmansyah ML, Jalil AA, Triwahyono S, Hamdan H, Salleh MM, Ahmad WFW, et al. Synthesis and characterization of fibrous silica ZSM-5 for cumene hydrocracking. Catalysis Science & Technology. 2016;6:5178-82.

[24] Abdulrasheed A, Jalil A, Hamid M, Siang T, Fatah N, Izan S, et al. Dry reforming of methane to hydrogen-rich syngas over robust fibrous KCC-1 stabilized nickel catalyst with high activity and coke resistance. International Journal of Hydrogen Energy. 2020;45:18549-61.
[25] Khusnun NF, Jalil AA, Abdullah TAT, Latip SSM, Hitam CNC, Fauzi AA, et al. Influence of TiO2 dispersion on silica support toward enhanced amine assisted CO2 photoconversion to methanol. Journal of CO2 Utilization. 2022;58:101901.
[26] Bahari MB, Mamat CR, Jalil AA, Shing LS, Hassan NS, Aziz FFA, et al. Enriching the methanol generation via CO2 photoconversion over the cockscomb-like fibrous silica copper. Fuel. 2022;328:125257.
[27] Siang TJ, Jalil AA, Fatah NAA, Chung ME. Tailoring Rh content on dendritic fibrous silica alumina catalyst for enhanced CO2 capture in catalytic CO2 methanation. Journal of Environmental Chemical Engineering. 2021;9:104616.
[28] Hussain MK, Khalid N, Tanveer M, Kebaili I, Alrobei H. Fabrication of CuO/MoO3 pn heterojunction for enhanced dyes degradation and hydrogen production from water splitting. International Journal of Hydrogen Energy. 2022;47:15491-504.
[29] Liu S, Yang Z, Zhao L, Zhang Y, Xing Y, Fei T, et al. Glucose-assisted combustion synthesis of oxygen vacancy enriched α-MoO3 for ethanol sensing. J Alloy Compd. 2022;902:163711.
[30] Izzudin NM, Jalil AA, Ali MW, Aziz FFA, Azami MS, Hassan NS, et al. Promoting a well-dispersion of MoO3 nanoparticles on fibrous silica catalyst via one-pot synthesis for enhanced photoredox environmental pollutants efficiency. Chemosphere. 2022;308:136456.
[31] Ibrahim M, Jalil A, Khusnun N, Fatah N, Hamid M, Gambo Y, et al. Enhanced n-hexane hydroisomerization over bicontinuous lamellar silica mordenite supported platinum (Pt/HM@ KCC-1) catalyst. International Journal of Hydrogen Energy. 2020;45:18587-99.
[32] Azami MS, Jalil AA, Hassan NS, Hussain I, Fauzi AA, Aziz MAA. Green carbonaceous material–fibrous silica-titania composite photocatalysts for enhanced degradation of toxic 2-chlorophenol. Journal of Hazardous Materials. 2021;414:125524.
[33] Myachina M, Gavrilova N, Nazarov V. Formation of Molybdenum Blue Nanoparticles in the Organic Reducing Area. Molecules. 2021;26:4438.
[34] Bahari MB, Jalil AA, Mamat CR, Hassan NS, Khusnun NF, Herrynaldi AR, et al. New insight into the mechanism of isomerization of C5–C7 alkanes over MoO3/FST. Molecular Catalysis. 2023;535:112873.
[35] Sawal MH, Jalil AA, Abdullah TAT, Khusnun NF, Hassan NS, Aziz FFA, et al. Si-Ti interaction in unique morphology of fibrous silica titania photoanode for enhanced photoelectrochemical water splitting. Energy Conversion and Management. 2022;274:116456.
[36] Hitam CNC, Jalil AA, Raji YO. Fabrication of Fibrous Silica Zinc (FSZn) Composite for Enhanced Photocatalytic Desulphurization. Topics in Catalysis. 2020;63:1169-81.
[37] Azami MS, Jalil AA, Aziz FFA, Hassan NS, Mamat CR, Izzudin NM. Influence of the nitrogen pots from graphitic carbon nitride with the presence of wrinkled silica-titania for photodegradation enhancement of 2-chlorophenol. International Journal of Hydrogen Energy. 2021.
[38] Aziz FFA, Jalil AA, Triwahyono S, Mohamed M. Controllable structure of fibrous SiO2–ZSM-5 support decorated with TiO2 catalysts for enhanced photodegradation of paracetamol. Applied Surface Science. 2018;455:84-95.
[39] Auepattana-aumrung C, Suriye K, Jongsomjit B, Panpranot J, Praserthdam P. Inhibition effect of Na+ form in ZSM-5 zeolite on hydrogen transfer reaction via 1-butene cracking. Catalysis Today. 2020;358:237-45.

[40] Rahman AFA, Jalil AA, Hamid MYS, Hussain I, Hassan NS, Khoja AH. Improved ethylbenzene suppression and coke-resistance on benzene methylation over metals doped fibrous silica-HZSM-5 zeolite. Molecular Catalysis. 2022;526:112370.
[41] Gao X, Chen C, Zhang W, Hong Y, Wang C, Wu G. Sulfated TiO2 supported molybdenum-based catalysts for transesterification of Jatropha seed oil: Effect of molybdenum species and acidity properties. Renewable Energy. 2022;191:357-69.
[42] Cruz MC, Sánchez-Velandia JE, Causíl S, Villa AL. Selective Synthesis of Perillyl Alcohol from β-Pinene Epoxide over Ti and Mo Supported Catalysts. Catalysis Letters. 2021;151:2279-90.
[43] Setiabudi HD, Jalil AA, Triwahyono S. Ir/Pt-HZSM5 for n-pentane isomerization: Effect of iridium loading on the properties and catalytic activity. Journal of Catalysis. 2012;294:128-35.
[44] Ma J, Qiang L-S, Wang J-F, Tang X-B, Tang D-Y. Effect of different synthesis methods on the structural and catalytic performance of SBA-15 modified by aluminum. Journal of Porous Materials. 2011;18:607-14.
[45] Lyu Y, Liu Y, Xu L, Zhao X, Liu Z, Liu X, et al. Effect of ethanol on the surface properties and n-heptane isomerization performance of Ni/SAPO-11. Applied Surface Science. 2017;401:57-64.
[46] Triwahyono S, Jalil AA, Ruslan NN, Setiabudi HD, Kamarudin NHN. C5–C7 linear alkane hydroisomerization over MoO3–ZrO2 and Pt/MoO3–ZrO2 catalysts. Journal of Catalysis. 2013;303:50-9.
[47] Chica A, Corma A, Miguel PJ. Isomerization of C5–C7 n-alkanes on unidirectional large pore zeolites: activity, selectivity and adsorption features. Catalysis Today. 2001;65:101-10.
[48] Noda LK, de Almeida RM, Probst LFD, Gonçalves NS. Characterization of sulfated TiO2 prepared by the sol–gel method and its catalytic activity in the n-hexane isomerization reaction. Journal of Molecular Catalysis A: Chemical. 2005;225:39-46.
[49] Hattori H. Solid Acid Catalysts: Roles in Chemical Industries and New Concepts. Topics in Catalysis. 2010;53:432-8.
[50] Al-Kandari H, Mohamed AM, Al-Kharafi F, Zaki MI, Katrib A. Modification of the catalytic properties of MoO2−x(OH)y dispersed on TiO2 by Pt and Cs additives. Applied Catalysis A: General. 2012;417-418:298-305.
[51] Matsuda T, Ohno T, Hiramatsu Y, Li Z, Sakagami H, Takahashi N. Effects of the amount of MoO3 on the catalytic properties of H2-reduced Pt/MoO3–SiO2 for heptane isomerization. Applied Catalysis A: General. 2009;362:40-6.
[52] Breitkopf C, Papp H, Li X, Olindo R, Lercher JA, Lloyd R, et al. Activation and isomerization of n-butane on sulfated zirconia model systems—an integrated study across the materials and pressure gaps. Physical Chemistry Chemical Physics. 2007;9:3600-18.
[53] Ruslan NN, Fadzlillah NA, Karim AH, Jalil AA, Triwahyono S. IR study of active sites for n-heptane isomerization over MoO3-ZrO2. Applied Catalysis A: General. 2011;406:102-12.
[54] Liu P, Wu M-Y, Wang J, Zhang W-H, Li Y-X. Hydroisomerization of n-heptane over MoP/Hβ catalyst doped with metal additive. Fuel Processing Technology. 2015;131:311-6.
[55] Parsafard N, Peyrovi MH, Parsafard N. Pt-HMS catalyst promoted with MoOx/ZrO2 mixed oxides for n-heptane isomerization: catalytic performance and kinetics. Reaction Kinetics, Mechanisms and Catalysis. 2017;120:231-46.

Mechanistic studies of lower temperature isomerization of n-heptane over fibrous silica molybdenum catalyst

M.B. Bahari[c], A.A. Jalil[a,b*], C.R. Mamat[c], N.S. Hassan[a,b], M.H. Razak[a], N.M. Izzudin[a], M.A.A. Aziz[a], N.F. Khusnun[b], M.A.H.Aziz[c], A.F.A. Rahman[b], W. Nabgan[d], Saravanan Rajendran[e]

[a] *Faculty of Chemical and Energy Engineering, Universiti Teknologi Malaysia, 81310 UTM Johor Bahru, Johor, Malaysia.*

[b] *Centre of Hydrogen Energy, Institute of Future Energy, Universiti Teknologi Malaysia, 81310 UTM Johor Bahru, Johor, Malaysia.*

[c] *Faculty of Science, Universiti Teknologi Malaysia, 81310 UTM Johor Bahru, Johor, Malaysia.*

[d] *Departament d'Enginyeria Química, Universitat Rovira i Virgili, Av Països Catalans 26, 43007, Tarragona, Spain*

[e] *Departamento de Ingeniería Mec´anica, Facultad de Ingeniería, Universidad de Tarapac´a, Avda. General Vel´asquez 1775, Arica, Chile*

**To whom correspondence should be addressed,*
Aishah Abdul Jalil (Ph.D.)
Tel: 60-7-5535581 Fax: 60-7-5536165
Email: aishahaj@utm.my

Abstract

Platinum (Pt) inclusion on fibrous silica molybdenum (FSMO) and MoO_3/KCC-1 catalysts has been prepared and utilized for the lower temperature (200-350 ºC) catalytic isomerization of n-heptane. The impact of Pt inclusion towards the structure, morphology, and acid distribution of catalysts was characterized by XRD, FTIR, N_2-physisorption, Py-IR, and H_2-IR. Compared with MoO_3/KCC-1, FSMO demonstrated superior MoO_3 dispersion and amount of Lewis acid site associated with the in-situ synthesis technique. Although Pt inclusion slightly lessened acid sites due to inevitable partial coverage by the Pt cluster, the considerably higher amount of Lewis acid sites compared to Brønsted and conjugated sufficiently for generating protonic acid sites for enriching the isomerization activity. In contrast to Pt/MoO_3/KCC-1 and undoped catalysts, Pt/FSMO achieved a superior conversion of 70.9% with 63.6% isomer yield at a low temperature of 250 ºC. The 28-h stability tests demonstrated that Pt/FSMO recorded stable isomerization activity, with a superior isomer yield (~48-52%) and inferior cracking yield (<3.0%) than Pt/MoO_3/KCC-1.

Keywords: n-C_7 isomerization; MoO_3-based catalysts; Platinum; Lewis acid; Protonic acid side

1.0 Introduction

Globally, comprehensive research and development initiatives have been undertaken to produce clean gasoline with low aromatics, olefins, sulphur, and high-octane numbers, in response to growing concerns over energy and environmental issues [1]. As a result, n-alkane isomerization has gained popularity as a safe and environmentally friendly method for enhancing gasoline quality [2]. This pathway allows n-alkanes with a linear carbon chain to be converted into branched isomers with a high research octane number (RON) [3, 4]. So far, tremendous effort has been put forth in researching light alkane isomerization since this compound processing has been industrialised. Yet, this technique has not been utilized for *n*-heptane and heavier alkanes due to the higher tendency of excessive development of cracking products as the conversion rate increases, leading to the deactivation of the catalyst due to the accumulation of coke on the surface's catalysts [5]. Hence, considering potential implementation, it is critical to look for relatively efficient and selective catalysts for heavy n-heptane isomerization while concurrently limiting cracking activities.

Bifunctional heterogeneous catalyst materials consisting of acidic supporting materials as well as hydrogenation/hydrogenation metal sites are among the popular catalysts used for the catalytic acid reaction [6, 7]. Both metallic and acidic functions influence the catalyst's properties and facilitate the alkane hydro-conversion. For instance, metal sites could generate carbonium ions via alkane dehydrogenation, a crucial intermediate species for initiating isomerization and cracking [8]. Once the acidity of the catalyst is mild, and the dehydrogenation activity of metal is substantial, a high yield of isomers is generated. In addition, when the dehydrogenation activity is more significant, unsaturated products are more hydrogenated, thus, inhibiting the escape acid-catalyzed skeleton rearrangement and cracking [9]. Throughout the scientific literature, *n*-alkane isomerization has made considerable use of

catalysts such as noble metals supported on microporous and mesoporous materials. In fact, it was found that the hydrogen atom spillover mechanism used by bifunctional heterogeneous catalysts could strongly induce isomerization [10]. Numerous acid-catalyzed reactions using various types of catalysts, like Pt/MoO_3 [11-13], Pt/WO_3-ZrO_2 [14], MoO_3/MSN [15], and Zn/HZSM-5 [10], have been explored for their spillover mechanisms.

Recently, the potential of the MoO_3 type catalysts has been extensively explored for a wide range of catalytic processes like methanation, olefin metathesis, alcohols oxidation, and isomerization accredited to MoO_3's exceptional features, including excellent stability and regeneration performance [16]. In addition, MoO_3 possessed both Lewis and Bronsted acid sites, which is crucial for *n*-alkane isomerization and provides superior selectivity for heptane isomerization compared to conventional catalysts. Incorporating second material as active sites into bifunctional catalysts has aroused considerable attention in recent years owing to the positive effects on isomerization performance, isomer selectivity, as well as stability. Second Noble materials like Pd and Pt have been extensively studied, attributed to their hydrogen spillover capability, boosting the isomerization activity. Indeed, the combination between Pt and MoO_3 in a hydrogen atmosphere can generate several active species, including H_xMoO_3 and MoO_2, that are utilized for isomerization [11, 17]. Previous work has demonstrated that incorporating Pt and MoO_3 into diverse supporting materials effectively improved n-heptane isomerization performance [11, 13]. Regrettably, it should be noted that there is a paucity of literature focusing on the usage of catalysts at low operating temperature.

Creating support with a dendrimer fibrous structure has recently received much attention [18]. This strategy can produce an ideal support material possessing vast surface area, tuneable pore volume, conveniently reachable inner surface, as well as superior thermal stability [19-21]. In fact, this approach has resulted in a positive effect on the catalytic activity of all catalytic pathways, including isomerization [4], methanation [22], cumene cracking [23],

and dry reforming [24]. According to the researchers, the improvement was attributable to the enhanced accessibility of active areas within this particular shape. Inspired by the previous study, we synthesized fibrous silica-molybdenum trioxide (FSMO) supported platinum (Pt) and assessed their capability in *n*-heptane isomerization at low reaction temperature for the first time. The fibrous silica in the Pt/FSMO catalyst induces Si-O-Mo formation to enhance Lewis acid site quantity, which will cause a growth in protonic acid site generation, thus enriching *n*-heptane isomerization activity. The physicochemical features of the studied catalysts were analysed in detail via XRD, N_2 physisorption and several in-situ IR analysis. The isomerization pathway over Pt/FSMO catalyst is also elucidated.

2.0 Experimental

2.1 MoO_3-based catalysts synthesis

Fibrous silica-molybdenum (FSMO) and KCC-1 were prepared corresponding to the microemulsion approach as detailed in the literature [25, 26]. In brief, a homogeneous solution consisting of CTAB and urea was acquired by mixing and stirring both chemicals in distilled water for 15 min (25ºC). Thereafter, butanol and toluene were poured into the mixture under continuous agitation at ambient temperature before being dopped with the specified amount of MoO_3 seed. The resulting mixture was further agitated at ambient temperature for two hours to guarantee TEOS was hydrolyzed entirely prior to the six-hour hydrothermal treatment in microwave irradiation (120 ºC, 400 W). Afterwards, the acquired solution was air-dried in an oven (24 h, 110 ºC) to eradicate the moisture before furnace-calcination (6 h, 550 ºC) to gain desired FSMO. On the contrary, for KCC-1 support production, TEOS was dropped along with

butanol and toluene before being treated with a similar condition for hydrothermal treatment, air-drying, and furnace-calcination.

The incipient wetness impregnation technique, as reported by Siang et al. [27], was applied in this work to generate Pt/FSMO and MoO_3/KCC-1 catalysts. For KCC-1 supported 10.0 wt%MoO_3 catalyst, a calculated amount of ammonium heptamolybdate ($[NH_4]_6Mo_7O_{24}$) as the metal precursor and KCC-1 support were separately dissolved in the deionized water prior to the impregnation step. After both solutions were mixed and agitated at ambient temperature for four hours, the resulting mixture was further air-dried in an oven (24 h, 110 ºC) and subsequently underwent furnace-calcination (6 h, 550 ºC), which yielded MoO_3/KCC-1. A similar approach as those stated earlier was employed to prepare Pt/FSMO using chloroplatinic acid hexahydrate ($H_2PtCl_6 \cdot 6H_2O$) as the metal precursor (0.1 wt%Pt) over FSMO support. For Pt/MoO_3/KCC-1 catalyst preparation, the sequential incipient wetness impregnation technique was employed by discretely dissolved $H_2PtCl_6 \cdot 6H_2O$ and as-synthesized MoO_3/KCC-1 in deionized water. Afterwards, both dissolved materials were combined, agitated, dried, and calcined, similar to those earlier impregnation steps to acquire Pt/MoO_3/KCC-1.

2.3 Characterizations of MoO_3-based catalysts

The crystalline structure of studied catalysts was assessed by X-ray diffractogram (2θ = 20-85°, step size = 0.02) on a Bruker Advance D8 diffractometer equipped with Cu Ka radiation (λ =0.154 nm, V = 40 kV, I = 40m A). The Barrett-Joyner-Halenda (BJH) and Brunauer-Emmet-Teller (BET) techniques were applied to measure the catalyst's surface area and pore properties using liquid nitrogen at -196 °C in a Beckman Coulter SA3100 unit. The one-hour-outgassed treatment was initially employed at 300 °C prior to the nitrogen adsorption

at 77 K for eradicating the moisture and contaminants. The functional groups of the studied catalysts were appraised via the FTIR-KBr approach at the range of 1600-400 cm^{-1} with 5 cm^{-1} resolutions on the FT-IR spectrometer unit (Agilent Cary 660). The acidity of studied catalysts was scrutinized through Py-IR adsorption on stainless-steel cells with two CaF2 windows sealed. Initially, the tested catalysts were pelletized before exposing them to 4 Torr of pyridine stream for a quarter-hour at 150 °C. Afterwards, the desorption of pyridine from tested catalysts was carried out at a different temperature within 150-350°C. H_2-IR adsorption was also operated in similar equipment for Py-IR adsorption. After activation treatment, the tested catalysts were cooled to room temperature before being subjected to 20 Torr of the hydrogen stream under rising temperature up to 350 °C. Temperature-programmed oxidation (TPO) was carried out in Mettler Toledo TGA/SDTA/851e Thermo-gravimetric unit to estimate the carbonaceous deposition on the surface of spent catalysts within the temperature of 10-900 °C.

2.4 n-C_7 Isomerization evaluation

The micro-catalytic pulse reactor was utilized to evaluate *n*-heptane isomerization within 200-350 °C. About 0.2 g of the studied catalyst was employed in the reactor, followed by exposure to the 100 ml min^{-1} of O_2 stream (1 h, 400 °C) and then 100 ml min^{-1} H_2 stream (3 h, 400 °C) as the pre-treatment step. Subsequently, the tested catalyst was cold down in a similar H_2 stream to reach 150 °C. After stabilizing and reaching the necessary conditions, about two µmol of n-C_7 was driven into the reactor filled with an H_2 stream (100 ml min^{-1}) to commence the isomerization process. An online gas chromatograph (Agilent 6090N, FID, HP-5), connected with a utilized micro-catalytic pulse reactor, scrutinized the isomerization product. The isomerization product was confined using N_2 (-196 °C) before being flash-evaporated into

the gas chromatograph system. The isomerization activity was estimated based on the conversion (X), yield (Y), and selectivity (S), as expressed in Eqs. (1)-(3).

$$X_i(\%) = \frac{\sum A_i - A_{r,i}}{\sum A_i} \times 100\% \quad (1)$$

$$S_i(\%) = \frac{A_i}{\sum A_i - A_{r,i}} \times 100\% \quad (2)$$

$$Y_i = \frac{X_i \times S_i}{100} \quad (3)$$

Where A_i = corrected chromatographic area for a specific product and $A_{r,i}$ = corrected chromatographic area for residual of n-heptane species, in weight percent unit.

3.0 Results and Discussion

3.1 Characterization analysis

XRD diffractograms for commercial MoO_3 and generated catalysts are shown in Figs. 1A-B. All of the prepared catalysts showed a clear peak at 2θ = 10°-70° on the plot. The XRD pattern of the MoO_3 catalyst demonstrated that it possesses an orthorhombic structure consistent with standard data (JCPDS Card No: 050508) [28]. The crystallite peaks corresponded to the MoO_3 witnessed at an angle of 2θ about 12.9° (020), 23.4° (110), 25.8° (040), 27.4° (021), 33.7° (111), 39.0° (041), 46.1° (200), and 49.4° (002) in FSMO and MoO_3/KCC-1 [29]. The inferior intensity of crystallite peaks of FSMO than MoO_3/KCC-1 catalyst, indicating that the in-situ synthesis strategy for generating FSMO promoted the well-distribution of Mo on the Si framework in comparison to MoO_3/KCC-1 prepared via the incipient wetness impregnation approach [30]. Furthermore, due to the small size of the Pt

species dispersed on the FSMO and MoO_3/KCC-1, possibly below than XRD detection limit, further explained for no visible diffraction peaks assignable to Pt species over Pt/FSMO and Pt/ MoO_3/KCC-1 [31].

The FTIR spectra (1400-400 cm^{-1}) of the functional groups owned by studied catalysts are depicted in Fig. 2. Evidently, all the studied catalysts displayed five identical IR bands ranging from 1095 cm^{-1} to 467 cm^{-1}. The absorption peaks appeared at a wavenumber of 1095 cm^{-1}, 956 cm^{-1}, 802 cm^{-1}, and 467 cm^{-1} are linked to the vibration of asymmetric Si-O-Si, external Si-OH, symmetric Si-O-Si, and bending Si-O-Si, respectively [32]. Meanwhile, absorption peaks identified at a wavenumber of 902 cm^{-1} overall studied catalysts signified weak Mo=O vibration [33, 34]. Following the modification of MoO_3 into FSMO, a drop in the intensity for the IR band at 956 cm^{-1} (external Si-OH vibration) for FSMO compared to MoO_3/KCC-1 suggesting that more replacement of hydrogen atom by Mo ions to form Si-O-Mo, associated with the alternately aligned SiO_2 and MoO_3 in the fibrous structure. As a consequence, this improvement could strengthen the interaction of MoO_3-SiO_2. This observation was also reported by Sawal et al. [35] and Hitam et al. [36]. Remarkably, the FTIR spectrum of FSMO was almost identical to that of Pt/FSMO, revealing no significant changes towards the silicate framework of FSMO after Pt incorporation. Apart from that, it is apparent from these FTIR spectra that most of the IR bands for FSMO and MoO_3/KCC-1 catalysts experienced a slight decrease in intensity compared to Pt-loaded catalysts, indicating the successful impregnation of Pt over the tested catalysts, creating new interaction between Pt and SiO_2.

Further investigation was performed using N_2 physisorption analysis to examine synthesized catalysts' textural properties; the results are presented in Fig. 3. As can be observed, all the prepared catalysts demonstrated a type IV isotherm profile with a typical H3 hysteresis loop, confirming the mesoporous structure characteristic of the synthesized catalysts (Fig. 3A)

[30]. In addition, in the absence of Pt element, both FSMO and MoO_3/KCC-1 catalysts exhibited comparable N_2 uptakes. However, when Pt was loaded onto the catalyst surface, the N_2 uptakes for Pt/MoO_3/KCC-1 increased substantially at higher relative pressure, while Pt/FSMO catalyst demonstrated an insignificant change. This result may be explained by the fact that high interaction between the Pt element and MoO_3 of Pt/MoO_3/KCC-1 reduced the pore blockage of the MoO_3 on the mesopore of the KCC-1 [36]. Besides, the total pore volume for MoO_3/KCC-1 catalyst increased after adding Pt (Table 1), which indirectly supported the earlier statement. Meanwhile, for Pt/FSMO catalyst, the pore volume was slightly decreased compared to the FSMO catalyst, suggesting the filling of Pt inside the FSMO mesopore [30].

Barrett-Joyner- Halenda (BJH) approach was applied to assess the average pore diameter, as shown in Fig. 3B. The BJH pore size distribution demonstrated the pore diameter of the synthesized catalysts placed within 3-40 (Å), showing the intrinsic of mesopores features. It is worth noting that the pore distribution of FSMO and KCC-1-supported MoO_3 catalysts were considerably grown by adding Pt, probably due to the high mesoporous of Pt that created inter-dendrimer distances [37]. For a better understanding of the textural properties of as-prepared catalysts, the results were tabulated and presented in Table 1. As noticed, the surface area for both FSMO (114.6 m^2/g) and MoO_3/KCC-1 (221.3 m^2/g) was reduced considerably after adding Pt, suggesting that pores of FSMO and MoO_3/KCC-1 catalysts were partially blocked by Pt particles [38]. This trend further inferred that the alteration of catalyst structure could lead to surface area changes.

The efficacy of the isomerization reaction was considerably linked to the number and intensity of the surface acidity in catalysts. Thus, Py-IR measurement was applied to assess the distribution of Lewis and Brønsted acidic sites over activated catalysts at different temperatures (150-250 ºC), and the Py-IR spectra are illustrated in Fig. 4. As can be seen, all of the studied catalysts disclosed three IR bands ranging within 1570-1420 cm^{-1}. It was noted that IR bands

spotted at 1454 cm^{-1} and 1539 cm^{-1} belonged to pyridinium ions adsorption on Lewis and Brønsted acid sites, respectively [39, 40]. In addition, the appearance of IR band at a wavenumber of 1488 cm^{-1} over all tested catalysts related to Brønsted and Lewis acid sites combination [41, 42]. Interestingly, by comparing FSMO and MoO_3/KCC-1, it was noticed that Lewis acid sites intensity for FSMO was considerably higher than KCC-1 supported MoO_3 catalysts, possibly ascribed to the more replacement of -H (from Brønsted) by Mo ions in forming Si-O-Mo (Lewis acid sites), resulted from the fibrous framework, in line with FTIR finding. The decline in Lewis and Brønsted acid site intensity was witnessed after Pt was impregnated onto FSMO and MoO_3/KCC-1, suggesting the inevitable partial coverage of acidic sites by the Pt cluster. A comparable phenomenon was claimed by Setiabudi et al. [43] and Teh et al. [5] during the isomerization over Ir/Pt-HZSM5 and Pt/MoO_3-HBEA catalysts, respectively.

The impact of outgassed temperature (150-350 ºC) towards the distribution of acidic sites on studied catalysts is also elucidated in Fig. 4. The pyridine molecules adsorbed on weak acid sites typically desorbed at a lower temperature whilst higher outgassing temperature is required for desorbing pyridine molecules for strong acid sites. All tested catalysts appeared to demonstrate intense interaction between pyridine and acidic sites at 150 ºC and remained firm at the outgassing temperature of 150 ºC. The considerable decline in the intensity of acidic sites for all studied catalysts was evidenced along with the rising outgassing temperature of up to 350 ºC, signifying that weak-to-moderate Brønsted and Lewis acid sites are dominantly located on those catalysts. This outcome also accords with the trends observed by other studies by Fatah et al. [15] and Ma et al. [44] during the Py-IR evaluation over Pt/MSN, MoO_3/MSN, and Al/SBA catalysts, respectively. Previous studies on isomerization have noted that the more significant amount and intensity of acid sites of catalysts favour cracking instead of

isomerization reaction [5, 45]. Thus, the optimum amount with moderate acid sites is preferable for enhanced isomerization.

Fig.5 disclosed the Py-IR spectra in 1600-1400 cm^{-1} when the pyridine pre-adsorbed catalysts were heated in H_2 gas at elevated temperatures. The heating of all catalysts under H_2 gas exposure modified the intensity of Lewis and Bronsted acid sites at 1446 cm^{-1} and 1538 cm^{-1}, respectively. Particularly, the intensity of Lewis acid sites declined with the simultaneous rise in the Bronsted acid sites, indicating the formation of protonic acid sites from hydrogen atoms spillover [4]. In general, protonic acid sites formed through interconversion of the Lewis acid sites. In this study, the protonic acid site formation rate is higher in all catalysts at lower temperatures (250-300 °C), as presented in Fig. 6. For FSMO and MoO_3/KCC-1, the formation of protonic acid sites was probably due to the interaction of the Mo atom with the proton in the form (MoO_x)-$(H_y)^+$) that generated from releasing of the electron by atomic hydrogen, as similarly reported by previous studies [15]. Interestingly, adding Pt into both catalysts significantly increased the protonic acid site formation rate, especially at low operating temperatures. These results indicated that Pt heightened the interaction of the hydrogen atom with the surface of FSMO and MoO_3/KCC-1. This phenomenon has also been observed in Pt/WO_3-ZrO_2 catalysts by Triwahyono et al. [46].

3.2 n-C_7 Isomerization performance

Fig. 7 depicts the isomerization activity of FSMO, MoO_3/KCC-1, Pt/FSMO, and Pt/MoO_3/KCC-1 in *n*-heptane isomerization within 200-350 ºC. Notably, all catalysts suffered a decrement in the yield of isomers along with the rise in operating temperature, which attained optimum yield at 200-250 ºC and decreased above 250 ºC. This trend was associated with the domination of cracking reaction compared to heptane isomerization at a higher temperature. It

is interesting to note that FSMO presented a superior *n*-heptane conversion (53-55%) and yield of isomers (46-52%) compared to MoO_3/KCC-1, regardless of reaction temperature owing to the considerably greater average pore size of FSMO (19.8 nm > 12.4 nm), as provided in Table 1. The enlargement in pore size was believed to minimize the transport restriction throughout the catalysts as well as improve the diffusion steps [47, 48]. Additionally, the high isomerization activity of FSMO than MoO_3/KCC-1 was probably related to possessing a moderate amount of weak Bronsted acid sites. This finding is accorded with the result from Py-IR with different outgassing temperatures (Fig. 4), which showed that FSMO possessed a lower amount of Bronsted acid sites than KCC-1 supported MoO_3 catalysts since there was more replacement of hydrogen atom (from Brønsted Si-OH) by Mo ions in forming Si-O-Mo (Lewis acid sites). Consequently, this domination facilitated the formation of the protonic acid site via H_2 dissociation and spillover, resulting in high isomerization activity. This trend was also evident from the experimental work of Triwahyono et al. [4], in which the modification of Y zeolite (HY) into fibrous silica@Y zeolite for C_5-C_7 isomerization.

Improvement in conversion and yield of isomer was noticed, especially at a lower temperature (<350 ºC) after incorporating Pt over FSMO and MoO_3/KCC-1 (Fig. 7). The results demonstrated that Pt/FSMO achieved optimal conversion of 70.9% with 63.6% isomer yield at a temperature of 250 ºC. Instead, Pt/MoO_3/KCC-1 recorded a maximum conversion of 61.7% with the yield of an isomer of 56.5% at 200 ºC. The enhancement in the isomerization activity after Pt addition, especially at low temperatures, was plausibly attributed to the considerably higher amount of Lewis acid sites than Brønsted and conjugated acid sites as demonstrated in Py-IR (cf. Fig. 4), appropriately sufficient in generating protonic acid sites for enriching the isomerization activity. Furthermore, this improvement could be linked to new active site species generated from the interaction of Pt-support lattice defects [5]. Thus, the addition of Pt over FSMO and MoO_3/KCC-1 could facilitate the activation of hydrogen

molecules via dissociation, enhancing the spillover process and thus enriching the formation of protonic acid sides and hydrides for generating more isomer products. Interestingly, the yield of cracking exhibited by Pt/FSMO is slightly lower compared to FSMO at 350 ºC, suggesting that Pt doped over FSMO effectively suppressed the binding interaction between FSMO and atomic hydrogen, thus enriching the formation of hydride ions that are responsible for the generation of the desired isomerization products [17]. In contrast, the high yield of cracking witnessed at 350 ºC for Pt/MoO_3/KCC-1 probably indicates that Pt incorporation could not restrain the binding interaction between support and spillover hydrogen atom, thus lowering the hydride generation. At low hydride availability, the hydrogen atoms' migration will occur slowly compared to the β-fission, favouring more cracking products than isomers [49].

Increased isomerization activity with the incorporation of Pt is also consistent with those of Al-Kandari et al. [50], who have evaluated the catalyst's isomerization activity over TiO_2-supported MoO_3. They found that Pt incorporation effectively improved the bifunctional metallic-acidic system of the MoO_3/TiO_2 catalyst, causing an improvement in *n*-heptane isomerization activity at 573 K. In different work, Matsuda and coworkers [51] highlighted that n-heptane isomerisation could be enhanced by introducing Pt over the reduced MoO_3 catalysts. The authors noticed that this effort could produce acidic molybdenum oxyhydride (MoO_xH_y), a crucial active site for enhancing the isomerization performance. Teh et al. [5] also discovered a significant improvement in n-heptane isomerization after incorporating Pt on the MoO_3-HBEA catalyst, accredited to the role of Pt in dissociating hydrogen molecule, suppressing the MoO_3-spillover hydrogen atom interaction, while enriched protonic acid sites quantity.

The stability performance of Pt/FSMO and Pt/MoO_3/KCC-1 in *n*-heptane isomerization under 28 h time-on-stream with intervals of 15 min for each dose was plotted in Fig. 8. Although Pt/MoO_3/KCC-1 recorded superior conversion (>~60.0%) as compared to Pt/FSMO, this catalyst experienced unsteady isomerization activity within 28 h reaction. This

phenomenon probably resulted from the high cracking side reaction, which could deactivate the catalysts as a consequence of high coke accumulation. On the contrary, Pt/FSMO recorded stable isomerization activity, especially with a better isomer yield (~48-52%) and a lower cracking yield (<3.0%). The temperature-programmed oxidation analysis was conducted to quantify the extent of carbonaceous deposition on the spent catalysts. As depicted in Fig. S1, it was evidenced that Pt/FSMO possessed an inferior amount of coke compared to Pt/MoO_3/KCC-1, further proving the stability of isomerization activity within 28 h reaction. This trend proves the efficient role of Pt in enhancing the Lewis acid site of the catalyst for generating essential protonic acid, minimizing the strong support-spillover hydrogen atom interaction, and assisting in lessening the coke accumulation via hydrogenation. Thus, it is noteworthy that Pt/FSMO catalysts have excellent potential for long-term isomerization reactions.

3.4 Proposed reaction pathway

Based on the characterizations and *n*-heptane isomerization test, as mentioned before, it can be evidenced that MoO_3 modification into the fibrous structure of support with silica (FSMO), along with the incorporation of Pt element, could enrich the generation of Lewis acid sites, thus, aiding in essential protonic acid sites generation at low temperature. This factor further explains the excellent performance of Pt/FSMO catalyst on *n*-heptane isomerization at a lower temperature. In order to comprehend the isomerization mechanism, the proposed reaction pathway for *n*-heptane isomerization over Pt/FSMO is clarified in Fig. 9.

At the initial pathway, the pre-treatment of Pt/FSMO in the H_2 stream resulted in the instigation of Pt-oxide into metallic Pt, the crucial hydrogen activation sites. The H_2 molecules adsorbed on metallic Pt were further dissociated into two species of hydrogen atoms. This

dissociation step is crucial in isomerization since it contributes to acid site generation, favouring the isomer generation instead of the cracking and polymerization of *n*-C_7 via ß-scission [4, 52]. After splitting, the produced hydrogen atom was spilt over onto the acidic surface of FSMO and further diffused towards the Lewis acid sites. The spilt over of hydrogen atoms then transferred an electron towards Lewis acid sites and bonded with Brønsted sites of FSMO for forming protonic acid site (B-H^+ species). The generated protonic acid sites then transferred protons to *n*-heptane, resulting in the formation of heptyl carbenium ion (*n*-C_7^+) species. Afterwards, the accepted proton in the carbenium ion was moved along the hydrocarbon chain, forming the iso-heptyl carbenium ion (*i*-C_7^+) species. Simultaneously, the electron confined by the Lewis acid sites was further reacted with another split hydrogen atom to become a hydride ion and attached to the Lewis acid site (L-H^-). Then, the produced L-H^- species further interacted with *i*-C_7^+ species contributing to the generation of the desired isomerization products. This proposed mechanism further proved that isomerization yield was strongly influenced by the protonic acid sites and hydrate ions created from H_2 dissociation in the presence of Pt. However, according to Hattori et al. [49], if there were excessive hydride species during the reaction, the concentration of carbenium ions would considerably drop, lowering the isomerization activity.

3.5 Comparative analysis

In order to evaluate the competency of our generated MoO_3-based catalysts, a comparative analysis (cf. Table 2) towards the reported MoO_3-based catalyst's activity over *n*-heptane isomerization was conducted. Fatah et al. [15] compared the isomerization activity of over MoO_3- and Pt- supported with MSN in the system consisting of H_2 or N_2 as the carrier. The high performance of MoO_3-supported with MSN conducted in the H_2 system was recorded

with mono- and di-branched iso-heptane, which yielded about 81.3 and 12.4%, respectively, resulting from $(MoO_x)^-(H_y)^+$ active sites formation. On the other hand, the authors claimed that the incompetence of the Pt- supported with MSN to generate protonic acid sites led to poor isomerization activity. The author also evaluated the isomerization performance over MoO_3 supported by KCC-1, incorporating the phosphorous element [16]. The generation of $(MoO_x)^-(H_y)^+$ active site along with the involvement of acidic centres from phosphorus inclusion and MoO_3, caused the improvement in the rate of n-heptane conversion.

In another effort, Ruslan et al. [53] investigated the role of the acid site of MoO_3-ZrO_2 catalysts toward n-heptane isomerization activity. Notably, the existence of the ZrO_2 tetragonal phase in the catalysts contributed to enhancement in the number of Lewis acid sites, easing active protonic acid site generation, thus responsible for the improvement of isomerization activity and stability. Nevertheless, the authors witness superior cracking activity compared to isomerization, which gradually increases with rising temperature from 300-400 ^oC. Besides, Matsuda et al. [51] emphasized the acid site's role and its impact on isomerization performance over Pt/MoO_3-SiO_2. They concluded that the isomerization selectivity of Pt/MoO_3-SiO_2 was enhanced from 88.7-97.8% by raising the amount of MoO_3 employed from 20-100wt%, related to the growth in the number of acid sites. Meanwhile, the cracking selectivity of Pt/MoO_3-SiO_2 was significantly reduced from 10.7% to 1.9% with the rising MoO_3 loading.

Liu et al. [54] stated that HBEA zeolite-supported molybdenum phosphide (MoP) demonstrated superior isomerization selectivity (67.8%) compared to tungsten phosphide supported on Hβ (50.1%) and HMCM22 (64.2%). The authors also proposed that doping Ce, Ni, and Cr elements over MoP/Hβ substantially enriched the activity with Cr-promoted catalyst promoted the superior isomerization selectivity around 73.1%, owing to the increment in the density of strong acid sites of MoP/Hβ. Works by Sakagami et al. [11] and Parsafard et al. [55] revealed a positive impact towards isomerization activity over MoO_3 and ZrO_2-HMS catalysts,

respectively, accredited to the presence of Pt, which enhances protonic acid site generation via H_2 dissociation and spillover phenomenon. This trend is in accordance with our findings. However, the negative impact of Pt incorporation was experienced by Triwahyono et al. [46] over MoO_3-ZrO_2. The authors justified that although Pt addition improved the hydrogen adsorption rate, Pt addition has caused the intensification of Lewis acid sites instead of forming more active protonic aicd sides, consequently lowering the isomerization activity.

Table 2 shows that our generated catalysts exhibited better or comparably to other MoO_3-based catalysts utilized for the isomerization of n-heptane, especially in conversion and isomerization selectivity. Indeed, the inferior cracking selectivity of studied catalysts compared to the literature indicates that all generated catalysts are favoured to isomerization activity compared to cracking. The outstanding performance of these generated catalysts, despite the absence of Pt, is ascribed to the fibrous silica morphology, which contributes to the formation of more Si-O-Mo for enriching Lewis acid sites quantity, causing growth in protonic acid sites generation, hence, enhancing the isomerization activity. Moreover, after Pt was doped, the enhancement of the Lewis acid site of the catalyst for generating essential protonic acid was evidenced, assisting in suppressing the strong support-spillover hydrogen atom interaction and lowering the coke accumulation. Thus, isomerization activity improved, especially at the lower reaction temperature.

4.0 Conclusion

This study appraised and compared the impact of Pt inclusion on physiochemical characteristics and isomerization activity of synthesized MoO3-based catalysts (FSMO and MoO3/KCC-1). XRD results indicated that the in-situ synthesis strategy effectively improved

the distribution of Mo particles in the Si framework than via incipient wetness impregnation. Additionally, the in-situ synthesis strategy promotes Si-O-Mo formation, associated with the alternately aligned SiO_2 and MoO_3 in the fibrous structure, strengthening MoO_3-SiO_2 interaction, as proved in FTIR analysis. Consequently, Py-IR analysis revealed that Lewis acid sites intensity for FSMO was considerably higher than KCC-1 supported MoO_3 catalyst, ascribed to the more replacement of -H (from Brønsted) by Mo ions in forming Si-O-Mo (Lewis acid sites). Nevertheless, it is noteworthy that Pt inclusion over FSMO and MoO_3/KCC-1 lessened those acid sites owing to the inevitable partial coverage by the Pt cluster.

The isomerization tests revealed enlargement in pore size, and the possession of a moderate amount of weak Bronsted acid sites contributed to the superior n-heptane conversion (53-55%) and yield of isomers (46-52%) for FSMO compared to MoO_3/KCC-1, regardless of reaction temperature. Meanwhile, incorporating Pt over FSMO and MoO_3/KCC-1 improved the conversion and yield of isomer, especially at a lower temperature (<350 ºC), by achieving optimal conversion of 70.9% with 63.6% isomer yield at a temperature of 250 ºC. At the same time, Pt/MoO_3/KCC-1 recorded a maximum conversion of 61.7% with the yield of an isomer of 56.5% at 200 ºC. This trend was plausibly accredited to the considerably more significant amount of Lewis than Brønsted and conjugated acid sites, sufficient to generate protonic acid sites for enriching the isomerization activity. Pt/FSMO recorded stable isomerization activity within 28 h, with a better isomer yield and a lower cracking yield than Pt/MoO_3/KCC-1 due to the efficient role of Pt in lessening the coke accumulation via hydrogenation. The findings of this study demonstrated the potential of Pt/FSMO as the catalyst for isomerization reactions.

Conflict of Interest

The authors hereby declare no conflict of interest for the research work reported in this manuscript.

Authorship contribution

M.B. Bahari: Project administration, Visualization, Writing - Original Draft, Methodology, **A.A. Jalil:** Project administration, Funding acquisition, Conceptualization, Visualization, Supervision, **N.S. Hassan:** Visualization, Writing - Original Draft, **MH Razak:** Investigation**,** Formal analysis, **N.M. Izzudin:** Investigation**,** Formal analysis, **NF. Khusnun:** Visualization, Writing - Original Draft**, M.A.H. Aziz**: Investigation**,** Formal analysis, **A.F.A. Rahman:** Investigation**,** Formal analysis, **W. Nabgan:** Investigation**,** Formal analysis, **Saravanan Rajendran:** Investigation**,** Formal analysis,

Acknowledgement

We are grateful for the financial support from Universiti Teknologi Malaysia (UTM) for the UTM Fundamental Research (No.22H51) and Professional Development Research University grant (No. 05E72).

References

[1] Smolikov MD, Shkurenok VA, Bikmetova LI, Prosvirin IP, Gulyaeva TI, Bukhtiyarov AV, et al. Effect of hydrogen reduction and palladium promotion of tungstate-modified zirconia on isomerization of heptane. Molecular Catalysis. 2022;529:112527.

[2] Ali NS, Alismaeel ZT, Majdi HS, Salih HG, Abdulrahman MA, Saady NMC, et al. Modification of SBA-15 mesoporous silica as an active heterogeneous catalyst for the hydroisomerization and hydrocracking of n-heptane. Heliyon. 2022;8:e09737.
[3] Saginayev A, Dosmurzina E, Apendina A, Dossanova B, Imangaliyeva B. Development of individual approaches to the use of the gasoline fraction as a raw material for the process of hydrocatalytic isomerization. Materials Science for Energy Technologies. 2022.
[4] Triwahyono S, Jalil AA, Izan SM, Jamari NS, Fatah NAA. Isomerization of linear C5–C7 over Pt loaded on protonated fibrous silica@Y zeolite (Pt/HSi@Y). Journal of Energy Chemistry. 2019;37:163-71.
[5] Teh LP, Setiabudi HD, Sidik SM, Annuar NHR, Jalil AA. Synergic role of platinum (Pt) and molybdenum trioxide (MoO_3) promoted HBEA zeolite towards n-heptane isomerization. Materials Chemistry and Physics. 2021;263:124406.
[6] Ono Y. A survey of the mechanism in catalytic isomerization of alkanes. Catalysis Today. 2003;81:3-16.
[7] Samad JE, Blanchard J, Sayag C, Louis C, Regalbuto JR. The controlled synthesis of metal-acid bifunctional catalysts: The effect of metal: acid ratio and metal-acid proximity in Pt silica-alumina catalysts for n-heptane isomerization. Journal of Catalysis. 2016;342:203-12.
[8] Blomsma E, Martens J, Jacobs P. Isomerization and hydrocracking of heptane over bimetallic bifunctional PtPd/H-beta and PtPd/USY zeolite catalysts. Journal of Catalysis. 1997;165:241-8.
[9] Sabyrov K, Musselwhite N, Melaet G, Somorjai GA. Hydroisomerization of n-hexadecane: remarkable selectivity of mesoporous silica post-synthetically modified with aluminum. Catalysis Science & Technology. 2017;7:1756-65.
[10] Triwahyono S, Jalil AA, Mukti RR, Musthofa M, Razali NAM, Aziz MAA. Hydrogen spillover behavior of Zn/HZSM-5 showing catalytically active protonic acid sites in the isomerization of n-pentane. Applied Catalysis A: General. 2011;407:91-9.
[11] Sakagami H, Ohno T, Takahashi N, Matsuda T. The effects of Na loading on catalytic properties of H_2-reduced Pt/MoO_3 for heptane isomerization. Journal of Catalysis. 2006;241:296-303.
[12] Triwahyono S, Jalil AA, Timmiati SN, Ruslan NN, Hattori H. Kinetics study of hydrogen adsorption over Pt/MoO_3. Applied Catalysis A: General. 2010;372:103-7.
[13] Matsuda T, Sakagami H, Takahashi N. H_2-reduced Pt/MoO_3 as a selective catalyst for heptane isomerization. Catalysis Today. 2003;81:31-42.
[14] Cheng TX, Kabashima H, Hattori H. Effects of hydrogen and hydrogen sulfide on cumene cracking catalyzed by Pt/WO_3-ZrO_2. Control of acidic and metallic functions. Reaction Kinetics and Catalysis Letters. 2000;69:201-7.
[15] Fatah NAA, Triwahyono S, Jalil AA, Ahmad A, Abdullah TAT. n-Heptane isomerization over mesostructured silica nanoparticles (MSN): Dissociative-adsorption of molecular hydrogen on Pt and Mo sites. Applied Catalysis A: General. 2016;516:135-43.
[16] Fatah NAA, Triwahyono S, Jalil AA, Salamun N, Mamat CR, Majid ZA. n-Heptane isomerization over molybdenum supported on bicontinuous concentric lamellar silica KCC-1: Influence of phosphorus and optimization using response surface methodology (RSM). Chemical Engineering Journal. 2017;314:650-9.
[17] Matsuda T, Uchijima F, Sakagami H, Takahashi N. H_2-reduction of Pt/MoO_3 to MoO_x with a large surface area and its catalytic activities for the conversions of heptane and propan-2-ol. Physical Chemistry Chemical Physics. 2001;3:4430-6.
[18] Izan SM, Jalil AA, Hitam CKNLCK, Nabgan W. Influence of nitrate and phosphate on silica fibrous beta zeolite framework for enhanced cyclic and noncyclic alkane isomerization. Inorganic Chemistry. 2020;59:1723-35.

[19] Aziz FFA, Jalil AA, Hassan NS, Hitam CNC, Rahman AFA, Fauzi AA. Enhanced visible-light driven multi-photoredox Cr(VI) and p-cresol by Si and Zr interplay in fibrous silica-zirconia. Journal of Hazardous Materials. 2021;401:123277.
[20] Aziz MAH, Jalil AA, Siang TJ, Hussain I, Rahman AFA, Hamdan H. Abundant Lewis acidic sites of peculiar fibrous silica zeolite X enhanced toluene conversion in side chain toluene methylation. Fuel. 2021;305:121432.
[21] Fauzi A, Jalil A, Mohamed M, Triwahyono S, Jusoh N, Rahman A, et al. Altering fiber density of cockscomb-like fibrous silica–titania catalysts for enhanced photodegradation of ibuprofen. Journal of Environmental Management. 2018;227:34-43.
[22] Siang TJ, Jalil AA, Hamid MYS. Bifunctional metal-free KAUST Catalysis Center 1 (KCC-1) as highly active catalyst for syngas production via methane partial oxidation. Materials Today Chemistry. 2022;23:100684.
[23] Firmansyah ML, Jalil AA, Triwahyono S, Hamdan H, Salleh MM, Ahmad WFW, et al. Synthesis and characterization of fibrous silica ZSM-5 for cumene hydrocracking. Catalysis Science & Technology. 2016;6:5178-82.
[24] Abdulrasheed A, Jalil A, Hamid M, Siang T, Fatah N, Izan S, et al. Dry reforming of methane to hydrogen-rich syngas over robust fibrous KCC-1 stabilized nickel catalyst with high activity and coke resistance. International Journal of Hydrogen Energy. 2020;45:18549-61.
[25] Khusnun NF, Jalil AA, Abdullah TAT, Latip SSM, Hitam CNC, Fauzi AA, et al. Influence of TiO_2 dispersion on silica support toward enhanced amine assisted CO_2 photoconversion to methanol. Journal of CO_2 Utilization. 2022;58:101901.
[26] Bahari MB, Mamat CR, Jalil AA, Shing LS, Hassan NS, Aziz FFA, et al. Enriching the methanol generation via CO_2 photoconversion over the cockscomb-like fibrous silica copper. Fuel. 2022;328:125257.
[27] Siang TJ, Jalil AA, Fatah NAA, Chung ME. Tailoring Rh content on dendritic fibrous silica alumina catalyst for enhanced CO_2 capture in catalytic CO_2 methanation. Journal of Environmental Chemical Engineering. 2021;9:104616.
[28] Hussain MK, Khalid N, Tanveer M, Kebaili I, Alrobei H. Fabrication of CuO/MoO_3 pn heterojunction for enhanced dyes degradation and hydrogen production from water splitting. International Journal of Hydrogen Energy. 2022;47:15491-504.
[29] Liu S, Yang Z, Zhao L, Zhang Y, Xing Y, Fei T, et al. Glucose-assisted combustion synthesis of oxygen vacancy enriched α-MoO_3 for ethanol sensing. Journal Alloy Compound. 2022;902:163711.
[30] Izzudin NM, Jalil AA, Ali MW, Aziz FFA, Azami MS, Hassan NS, et al. Promoting a well-dispersion of MoO_3 nanoparticles on fibrous silica catalyst via one-pot synthesis for enhanced photoredox environmental pollutants efficiency. Chemosphere. 2022;308:136456.
[31] Ibrahim M, Jalil A, Khusnun N, Fatah N, Hamid M, Gambo Y, et al. Enhanced n-hexane hydroisomerization over bicontinuous lamellar silica mordenite supported platinum (Pt/HM@ KCC-1) catalyst. International Journal of Hydrogen Energy. 2020;45:18587-99.
[32] Azami MS, Jalil AA, Hassan NS, Hussain I, Fauzi AA, Aziz MAA. Green carbonaceous material–fibrous silica-titania composite photocatalysts for enhanced degradation of toxic 2-chlorophenol. Journal of Hazardous Materials. 2021;414:125524.
[33] Myachina M, Gavrilova N, Nazarov V. Formation of Molybdenum Blue Nanoparticles in the Organic Reducing Area. Molecules. 2021;26:4438.
[34] Bahari MB, Jalil AA, Mamat CR, Hassan NS, Khusnun NF, Herrynaldi AR, et al. New insight into the mechanism of isomerization of C_5–C_7 alkanes over MoO_3/FST. Molecular Catalysis. 2023;535:112873.

[35] Sawal MH, Jalil AA, Abdullah TAT, Khusnun NF, Hassan NS, Aziz FFA, et al. Si-Ti interaction in unique morphology of fibrous silica titania photoanode for enhanced photoelectrochemical water splitting. Energy Conversion and Management. 2022;274:116456.
[36] Hitam CNC, Jalil AA, Raji YO. Fabrication of Fibrous Silica Zinc (FSZn) Composite for Enhanced Photocatalytic Desulphurization. Topics in Catalysis. 2020;63:1169-81.
[37] Azami MS, Jalil AA, Aziz FFA, Hassan NS, Mamat CR, Izzudin NM. Influence of the nitrogen pots from graphitic carbon nitride with the presence of wrinkled silica-titania for photodegradation enhancement of 2-chlorophenol. International Journal of Hydrogen Energy. 2021;48:6532-6545.
[38] Aziz FFA, Jalil AA, Triwahyono S, Mohamed M. Controllable structure of fibrous SiO_2–ZSM-5 support decorated with TiO_2 catalysts for enhanced photodegradation of paracetamol. Applied Surface Science. 2018;455:84-95.
[39] Auepattana-aumrung C, Suriye K, Jongsomjit B, Panpranot J, Praserthdam P. Inhibition effect of Na^+ form in ZSM-5 zeolite on hydrogen transfer reaction via 1-butene cracking. Catalysis Today. 2020;358:237-45.
[40] Rahman AFA, Jalil AA, Hamid MYS, Hussain I, Hassan NS, Khoja AH. Improved ethylbenzene suppression and coke-resistance on benzene methylation over metals doped fibrous silica-HZSM-5 zeolite. Molecular Catalysis. 2022;526:112370.
[41] Gao X, Chen C, Zhang W, Hong Y, Wang C, Wu G. Sulfated TiO2 supported molybdenum-based catalysts for transesterification of Jatropha seed oil: Effect of molybdenum species and acidity properties. Renewable Energy. 2022;191:357-69.
[42] Cruz MC, Sánchez-Velandia JE, Causíl S, Villa AL. Selective Synthesis of Perillyl Alcohol from β-Pinene Epoxide over Ti and Mo Supported Catalysts. Catalysis Letters. 2021;151:2279-90.
[43] Setiabudi HD, Jalil AA, Triwahyono S. Ir/Pt-HZSM5 for n-pentane isomerization: Effect of iridium loading on the properties and catalytic activity. Journal of Catalysis. 2012;294:128-35.
[44] Ma J, Qiang L-S, Wang J-F, Tang X-B, Tang D-Y. Effect of different synthesis methods on the structural and catalytic performance of SBA-15 modified by aluminum. Journal of Porous Materials. 2011;18:607-14.
[45] Lyu Y, Liu Y, Xu L, Zhao X, Liu Z, Liu X, et al. Effect of ethanol on the surface properties and n-heptane isomerization performance of Ni/SAPO-11. Applied Surface Science. 2017;401:57-64.
[46] Triwahyono S, Jalil AA, Ruslan NN, Setiabudi HD, Kamarudin NHN. C_5–C_7 linear alkane hydroisomerization over MoO_3–ZrO_2 and Pt/MoO_3–ZrO_2 catalysts. Journal of Catalysis. 2013;303:50-9.
[47] Chica A, Corma A, Miguel PJ. Isomerization of C_5–C_7 n-alkanes on unidirectional large pore zeolites: activity, selectivity and adsorption features. Catalysis Today. 2001;65:101-10.
[48] Noda LK, de Almeida RM, Probst LFD, Gonçalves NS. Characterization of sulfated TiO_2 prepared by the sol–gel method and its catalytic activity in the n-hexane isomerization reaction. Journal of Molecular Catalysis A: Chemical. 2005;225:39-46.
[49] Hattori H. Solid Acid Catalysts: Roles in Chemical Industries and New Concepts. Topics in Catalysis. 2010;53:432-8.
[50] Al-Kandari H, Mohamed AM, Al-Kharafi F, Zaki MI, Katrib A. Modification of the catalytic properties of $MoO_{2-x}(OH)_y$ dispersed on TiO_2 by Pt and Cs additives. Applied Catalysis A: General. 2012;417-418:298-305.
[51] Matsuda T, Ohno T, Hiramatsu Y, Li Z, Sakagami H, Takahashi N. Effects of the amount of MoO_3 on the catalytic properties of H_2-reduced Pt/MoO_3–SiO_2 for heptane isomerization. Applied Catalysis A: General. 2009;362:40-6.

[52] Breitkopf C, Papp H, Li X, Olindo R, Lercher JA, Lloyd R, et al. Activation and isomerization of n-butane on sulfated zirconia model systems—an integrated study across the materials and pressure gaps. Physical Chemistry Chemical Physics. 2007;9:3600-18.
[53] Ruslan NN, Fadzlillah NA, Karim AH, Jalil AA, Triwahyono S. IR study of active sites for n-heptane isomerization over MoO_3-ZrO_2. Applied Catalysis A: General. 2011;406:102-12.
[54] Liu P, Wu M-Y, Wang J, Zhang W-H, Li Y-X. Hydroisomerization of n-heptane over MoP/Hβ catalyst doped with metal additive. Fuel Processing Technology. 2015;131:311-6.
[55] Parsafard N, Peyrovi MH, Parsafard N. Pt-HMS catalyst promoted with MoO_x/ZrO_2 mixed oxides for n-heptane isomerization: catalytic performance and kinetics. Reaction Kinetics, Mechanisms and Catalysis. 2017;120:231-46.

List of Tables

Mechanistic studies of lower temperature isomerization of n-heptane over fibrous silica molybdenum catalyst

M.B. Bahari[c], A.A. Jalil[a,b*], C.R. Mamat[c], N.S. Hassan[a,b], M.H. Razak[a], N.M. Izzudin[a], M.A.A. Aziz[a], N.F. Khusnun[b], M.A.H.Aziz[c], A.F.A. Rahman[b], W. Nabgan[d], Saravanan Rajendran[e]

[a] *Faculty of Chemical and Energy Engineering, Universiti Teknologi Malaysia, 81310 UTM Johor Bahru, Johor, Malaysia.*

[b] *Centre of Hydrogen Energy, Institute of Future Energy, Universiti Teknologi Malaysia, 81310 UTM Johor Bahru, Johor, Malaysia.*

[c] *Faculty of Science, Universiti Teknologi Malaysia, 81310 UTM Johor Bahru, Johor, Malaysia.*

[d] *Departament d'Enginyeria Química, Universitat Rovira i Virgili, Av Països Catalans 26, 43007, Tarragona, Spain*

[e] *Departamento de Ingeniería Mec´anica, Facultad de Ingeniería, Universidad de Tarapac´a, Avda. General Vel´asquez 1775, Arica, Chile*

Table 1 Textural properties of catalysts

Catalyst	**Surface area (m^2/g)**	**Pore volume $x10^{-3}$ (cm^3/g)**	**Average pore size (nm)**
FSMO	114.6	5.2	19.8
Pt/FSMO	101.3	3.8	21.4
MoO_3/KCC-1	221.3	9.1	12.4
Pt/MoO_3/KCC-1	208.8	9.8	16.4

Table 2: Catalytic performance of MoO_3-based catalysts for *n*-heptane isomerization

Catalyst	T (°C)	Conversion (%)	Isomer selectivity (%)		Isomer Yield (%)	Cracking selectivity (%)	Ref.
			Mono-branched	Di-branched			
MoO_3/MSN	350	45.0	81.3	12.4	43.4	3.5	[15]
MoO_3/KCC-1	300	45.8	52.6	24.0	39.7	23.4	[16]
P/MoO_3/KCC-1	300	67.4	50.2	28.5	53.0	21.3	
Pt/MoO_3-SiO_2	250	57.3	97.5		-	2.1	[51]
MoO_3-ZrO_2	400	31.0	44.7		-	55.3	[53]
MoP/HMCM22	300	13.7	58.4	5.8	8.8	30.5	[54]
MoP/Hβ-40%	300	18.0	56.7	11.1	12.2	20.1	
Pt/MoO_3	300	53.1	90.9		-	9.1	[11]
Pt/Na-MoO_3	300	50.3	94.6		-	5.4	
Pt/Zr(x)-HMS	300	39.2	22.4	18.0	-	59.5	[55]
Pt–MoO_x/ZrO_2-HMS	300	53.1	43.6	22.8	-	33.6	
MoO_3-ZrO_2	300	-	44.7	-	13.8	-	[46]
Pt/MoO_3-ZrO_2	300	-	0	-	0	-	
FSMO	300	53.0	58.1	32.5	48.0	0.5	This work
Pt/FSMO	300	56.8	60.1	27.9	50.0	0.2	
MoO_3/KCC-1	300	47.5	61.4	25.5	41.2	0.5	
Pt/MoO_3/KCC-1	300	53.1	66.9	19.7	46.0	0.4	

List of Figures

Mechanistic studies of lower temperature isomerization of *n*-heptane over fibrous silica molybdenum catalyst

M.B. Bahari[c], A.A. Jalil[a,b*], C.R. Mamat[c], N.S. Hassan[a,b], M.H. Razak[a], N.M. Izzudin[a], M.A.A. Aziz[a], N.F. Khusnun[b], M.A.H.Aziz[c], A.F.A. Rahman[b], W. Nabgan[d], Saravanan Rajendran[e]

[a] *Faculty of Chemical and Energy Engineering, Universiti Teknologi Malaysia, 81310 UTM Johor Bahru, Johor, Malaysia.*

[b] *Centre of Hydrogen Energy, Institute of Future Energy, Universiti Teknologi Malaysia, 81310 UTM Johor Bahru, Johor, Malaysia.*

[c] *Faculty of Science, Universiti Teknologi Malaysia, 81310 UTM Johor Bahru, Johor, Malaysia.*

[d] *Departament d'Enginyeria Química, Universitat Rovira i Virgili, Av Països Catalans 26, 43007, Tarragona, Spain*

[e] *Departamento de Ingeniería Mec´anica, Facultad de Ingeniería, Universidad de Tarapac´a, Avda. General Vel´asquez 1775, Arica, Chile*

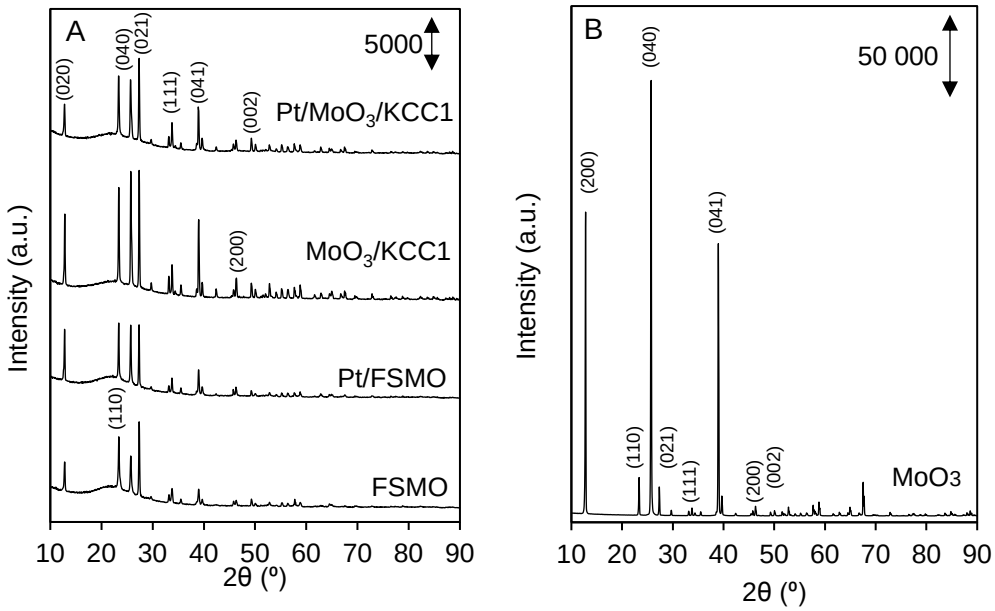

Fig. 1 XRD diffractogram for (A) MoO_3-based catalysts and (B) commercial MoO_3

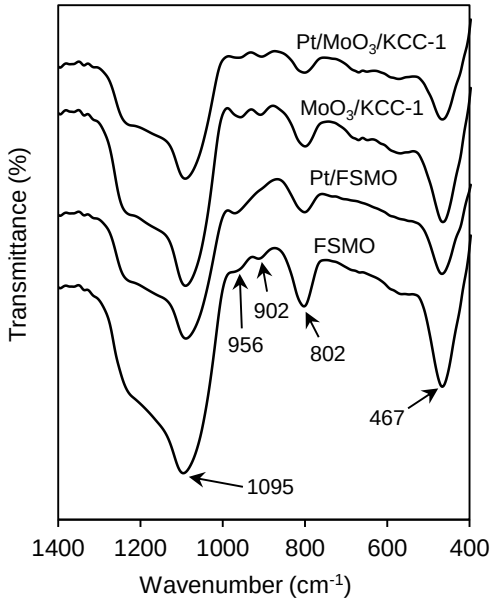

Fig. 2 FTIR spectra for all catalysts

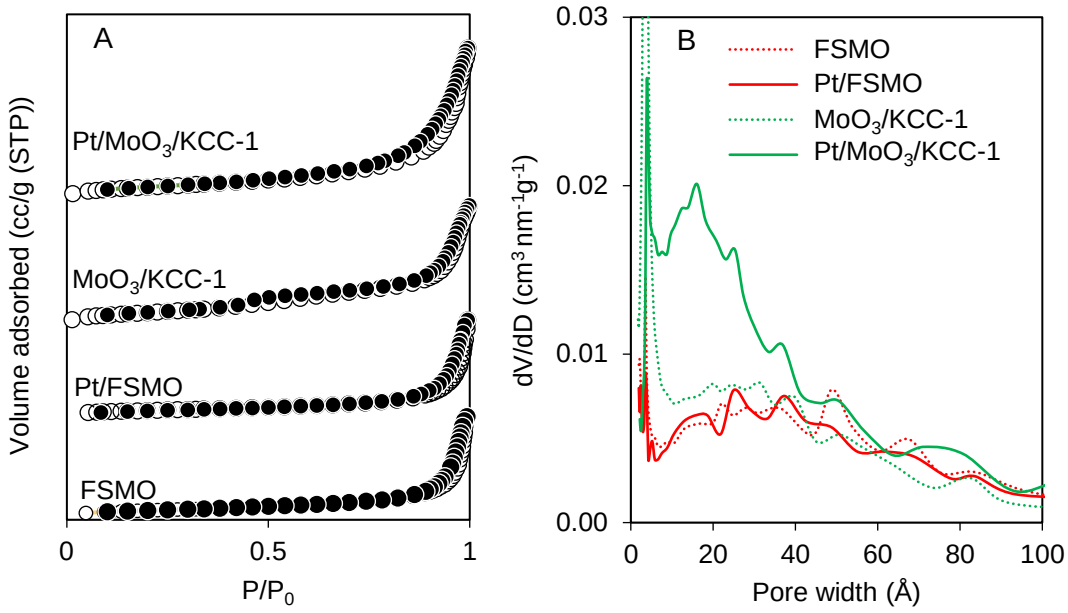

Fig. 3 N_2 adsorption-desorption and pore distribution for MoO_3-based catalysts

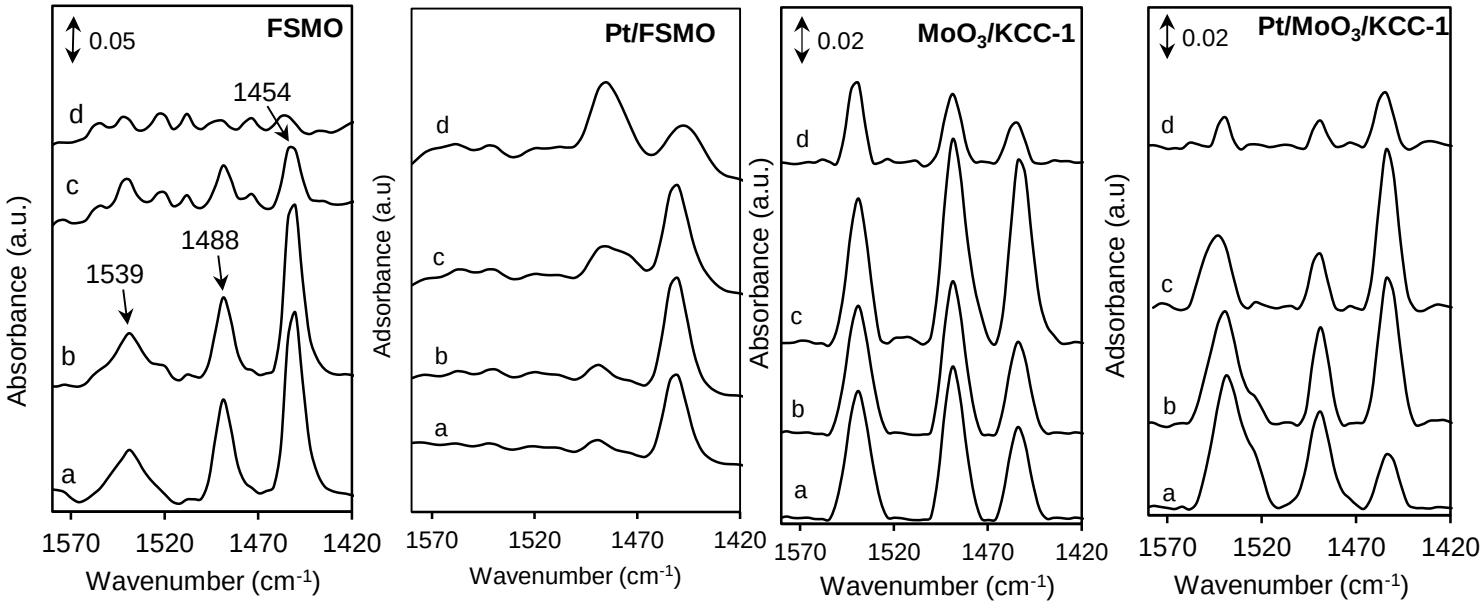

Fig 4 FTIR spectra of catalysts (a) after pyridine adsorption at 150 ºC, then outgassing at (b) 150 ºC (c) 250 ºC (d) 350 ºC

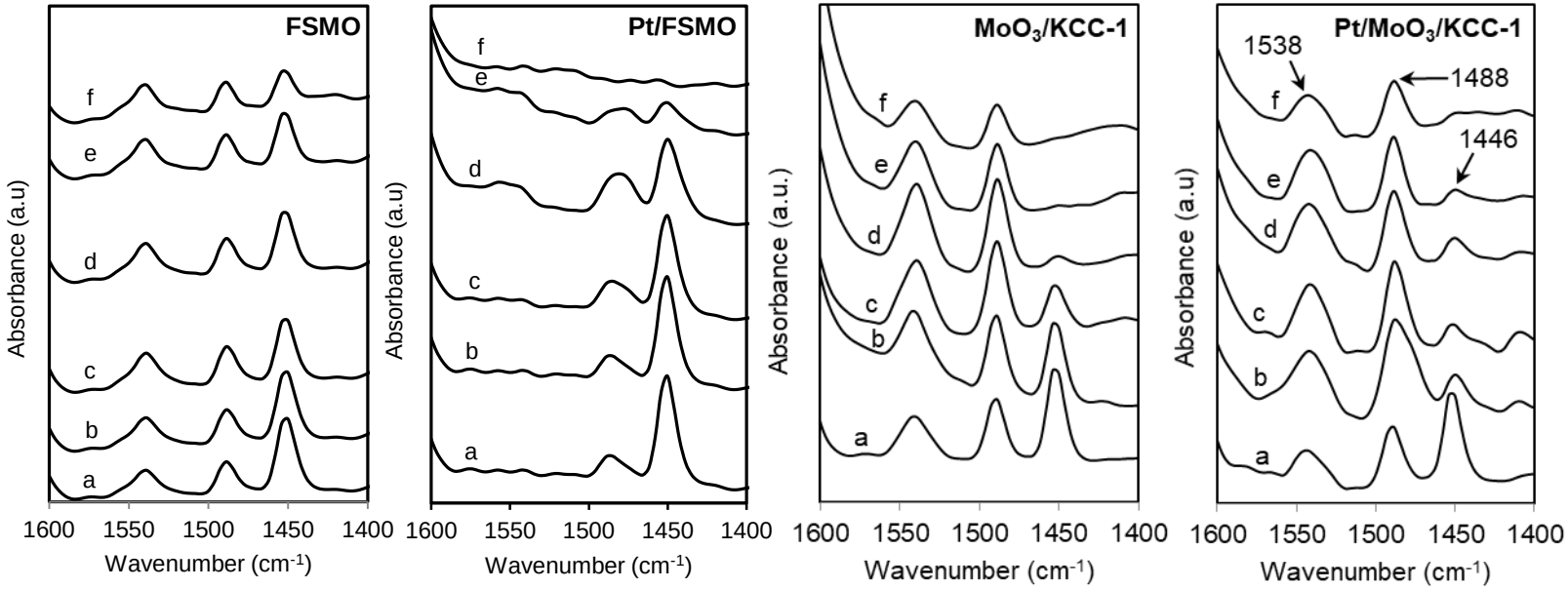

Fig. 5 Py-IR spectra of studied catalysts. Spectral variations induced by heating the pyridine-preadsorbed sample in H_2 at (a) room temperature (b) 100 ºC (c) 200 ºC (d) 250 ºC (e) 300 ºC (f) 350 ºC

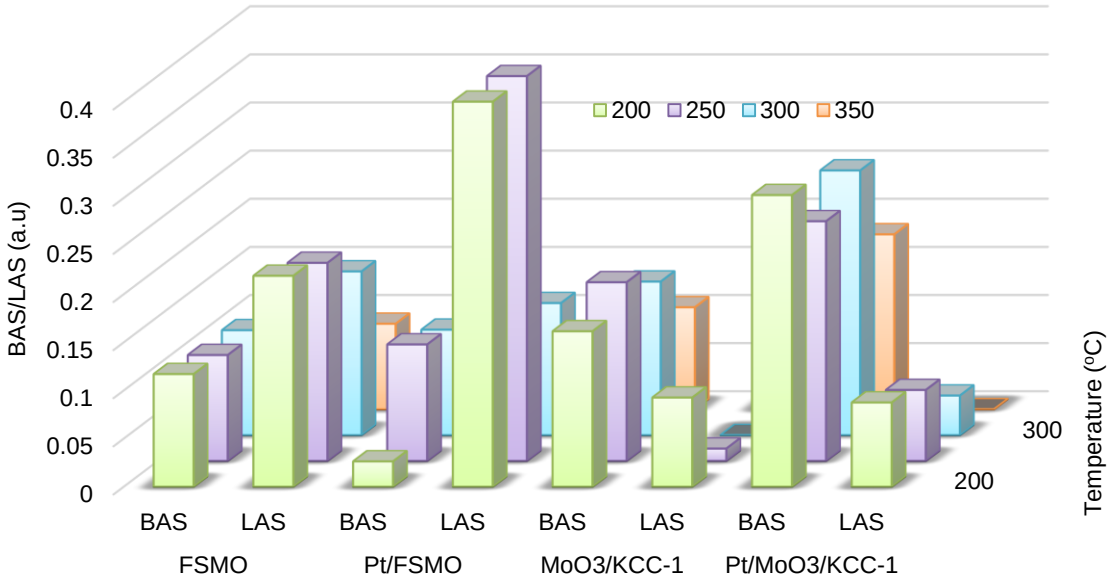

Fig. 6 Acid sites distribution of MoO_3-based catalysts detected by IR pyridine-preadsorbed and heated in hydrogen at elevated temperature (200-350°C)

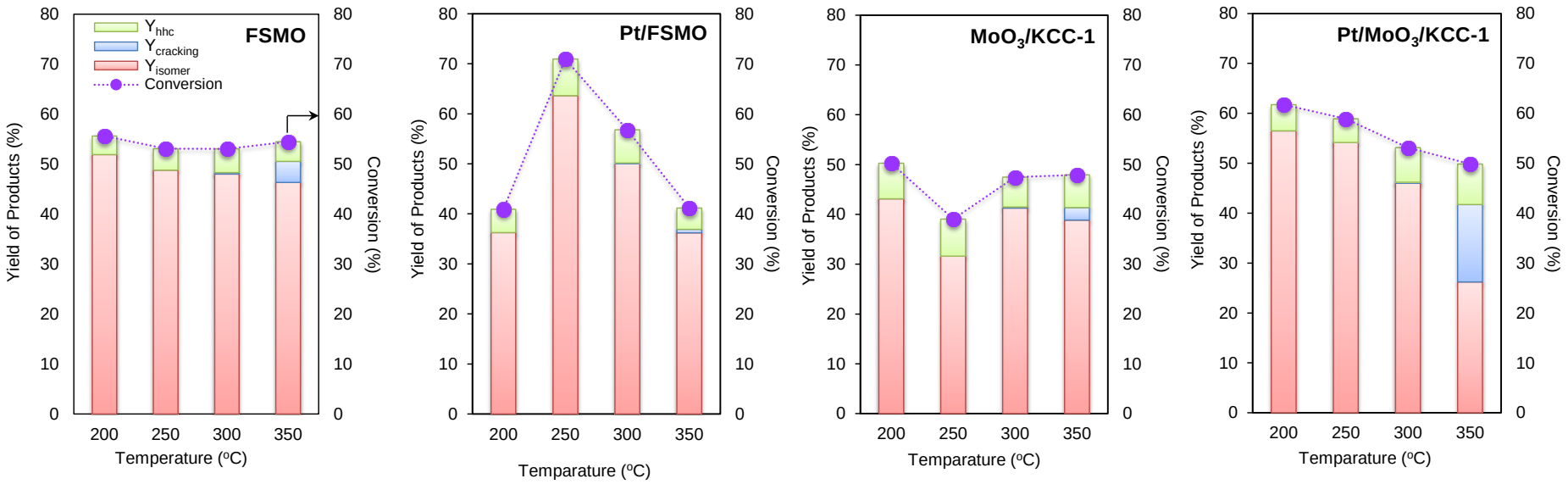

Fig. 7 *n*-heptane isomerization activity over MoO_3-based catalyst at elevated temperature (Y_{iso}= yield of isomer, $Y_{cracking}$ = Yield of cracking, and Y_{hhc} = Yield of higher hydrocarbon)

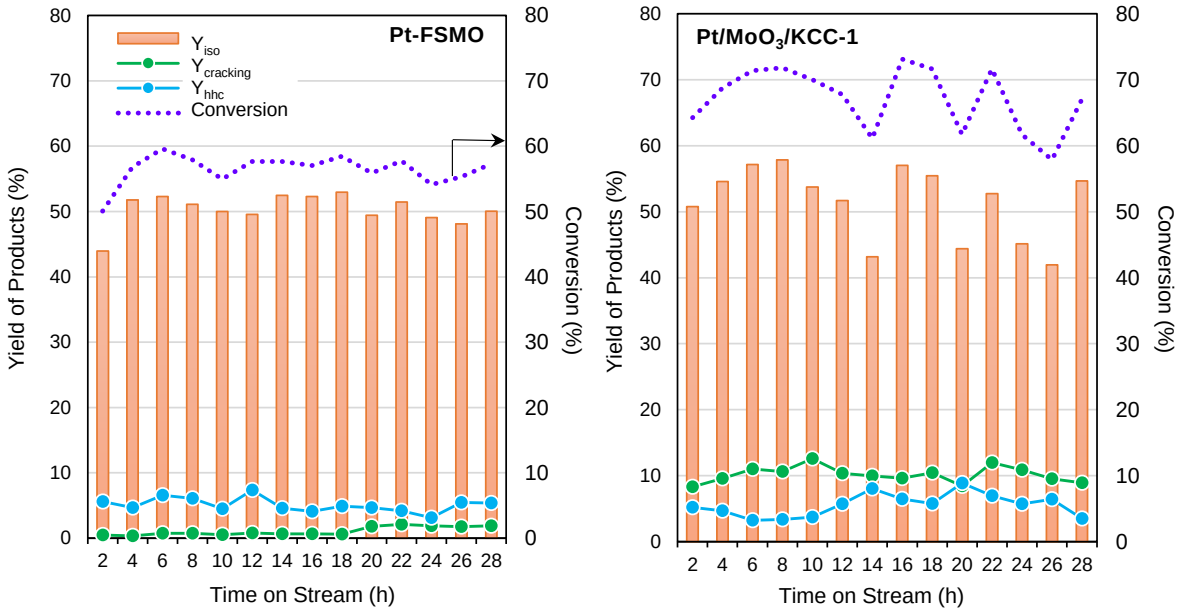

Fig. 8 Catalyst stability test under 28 h time-on-stream at 250 ºC, atmospheric pressure, and 0.2 g of catalyst. (2 µmol of n-C_7 + 100 ml min^{-1} H_2)

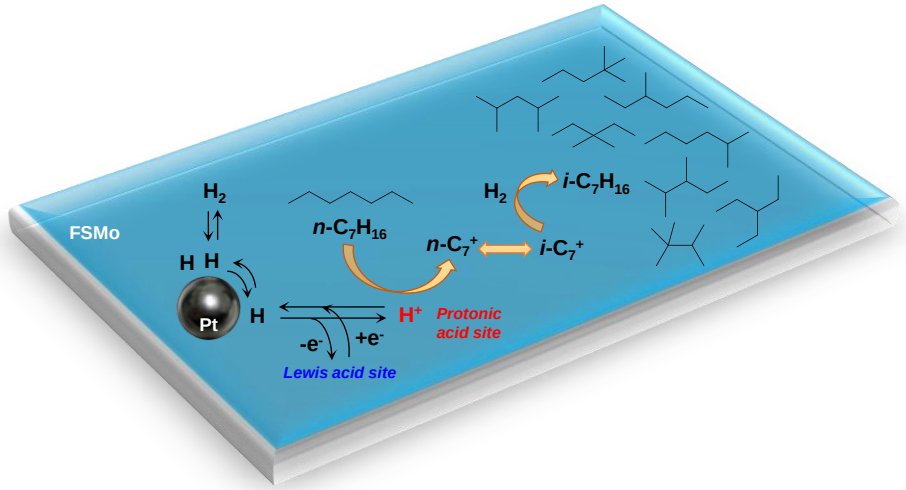

Fig. 9 Mechanism proposed for n-heptane isomerization over Pt/FSMO

Declaration of interests

☒The authors declare that they have no known competing financial interests or personal relationships that could have appeared to influence the work reported in this paper.

☐The authors declare the following financial interests/personal relationships which may be considered as potential competing interests: